Vol. 35 (2004) ACTA PHYSICA POLONICA B No 12

GENERAL CHARACTERISTICS OF HADRON–HADRON COLLISIONS*

W. Kittel

HEFIN, Radboud University of Nijmegen/NIKHEF
Toernooiveld 1, 6525 ED Nijmegen, The Netherlands

(Received October 4, 2004)

Soft multiparticle production in hadron-hadron collisions is reviewed with particular emphasis on its role as a standard for heavy-ion collisions at SPS and RHIC energies and as a bridge interpolating between the most simple e^+e^- and the most complex AA collisions.

PACS numbers: 12.38.Qk, 13.66.Bc, 13.85.Hd, 13.87.Fh

1. Single-particle (and resonance) inclusive spectra

1.1. Feynman-x and rapidity

Elastic scattering and diffraction dissociation lead to simple final states with relatively few particles. The larger part of the collisions leads to high particle multiplicities with complicated structure in highly-dimensional phase space. The first and most simple approach is then to study an all-inclusive density distribution in one of these dimensions.

Fig. 1.1(a) shows [1] the energy dependence of the invariant distribution

$$F(x) = \int \frac{E^*}{p^*_{\rm max}} \frac{d^2\sigma}{dx dp^2_{\rm T}} dp^2_{\rm T} \tag{1}$$

in the Feynman variable $x = p^*_{\parallel}/p^*_{\rm max}$, the component of the particle cms momentum in the beam direction, normalized to its maximum possible value, in K^+p collisions. The upper part (mind the change in scale) corresponds to positive particles except for identified protons, the lower part to π^--production. The large-$|x|$ region shows energy scaling and a fall-off of the distribution towards its tails which is steeper for the proton region (large

* Presented at the XLIV Cracow School of Theoretical Physics, Zakopane, Poland, May 28–June 6, 2004.

negative x) than for the K^+ region (large positive x). The large-$|x|$ scaling is in agreement with the early concept of limiting fragmentation [2] stating that at high enough energy, the fragmentation of beam or target is expected to reach an energy independent limit for particles produced with finite momentum in the rest frame of the fragmenting particle. Experimentally, this was convincingly shown to hold at ISR energies for pp collisions between $\sqrt{s} = 31$ and 53 GeV [3].

A scaling violation is, however, observed in the form of an increase of $F(x)$ with increasing beam momentum for the low-$|x|$ (central) region. An alternative variable, expanding the central region, is the rapidity $y = 0.5\ln[(E+p_{\|})/(E-p_{\|})]$. The energy dependence for the cms y-distribution for essentially the same data as above is shown in Fig. 1.1(b). The distribution widens with increasing energy. In the center, a plateau develops at high energies, reaching a width of about 3 rapidity units at 250 GeV/c beam momentum, and the density increases for all y.

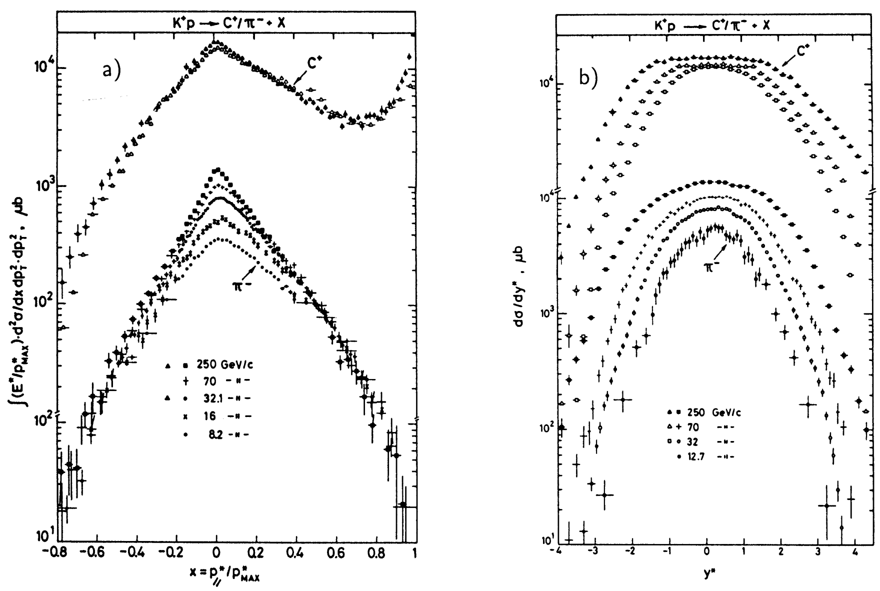

Fig. 1.1. (a) The invariant Feynman-x distribution for the inclusive reactions $K^+p \rightarrow C^+ + X$ and $K^+p \rightarrow \pi^- + X$ between 8.2 and 250 GeV/c; (b) the rapidity distribution for the same reactions between 12.7 and 250 GeV/c [1].

This low-$|y|$ increase with increasing energy is in contradiction to the early hypothesis of so-called Feynman scaling [4], based on the assumption that, asymptotically, interaction between two colliding hadrons occurs only through exchange of partons or parton systems of "wee" longitudinal momentum, *i.e.* of partons with a non-zero amplitude in both hemispheres.

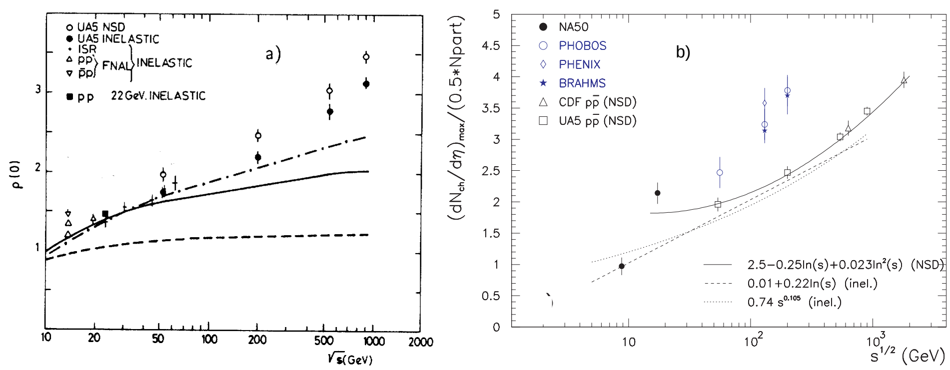

Fig. 1.2. (a) The central density $\rho(0)$ of the c.m. pseudo-rapidity distribution as a function of $\sqrt{s}$ [1]. The solid, dashed and dashed-dotted curves are DPM, Lund and FRITIOF. (b) The central density per participant pair for central heavy ion collisions at SPS and RHIC. The lines are fits to the $p\bar{p}$ data [13].

A lab momentum of 250 GeV/c corresponds to $\sqrt{s} = 22$ GeV, so not to an asymptotic energy. Therefore, in Fig. 1.2(a) the central pseudo-rapidity density $\rho(0) = (1/\sigma_{\text{inel}})[d\sigma/d\eta]_{\eta=0}$ is displayed versus $\sqrt{s}$ [1, 5, 6] up to 1800 GeV, but an upward curvature rather than Feynman scaling is observed. The lines correspond to quark string models, as examples for a first comparison. The single-string Lund model [7] does not reproduce the rise of the central pseudo-rapidity density in the energy range presented. The two-string model FRITIOF (with hard parton scattering) [8] and a two-string dual parton model (DPM) [9] agree reasonably well with the data up to $\sqrt{s}$=60 GeV, but underestimate the rise for higher energies.

So, Feynman scaling does not hold, but limiting fragmentation does, and it has turned out that this is the case in a much wider range of rapidities than originally proposed, and not only in hadron–hadron [5], but also in hadron–nucleus and nucleus–nucleus collisions [10, 11]. Fig. 1.3 shows that in these types of collisions, the particle density in the fragmentation region increases linearly with decreasing pseudorapidity $\eta - Y$ (Y being the beam rapidity) towards the central plateau. The range of this limiting fragmentation region increases with increasing energy, so that the width of the central plateau grows much slower than anticipated (see also W. Busza, these proceedings).

Abandoning Feynman scaling, Bialas and Jezabek [12] show that these features can be understood from a two-step process, where a number of color exchanges take place between two sets of partons (one in each of the colliding hadrons) which are *uniformly distributed in rapidity*, so not just "wee", and the color charges created this way then emit particle clusters by bremsstrahlung or color string decay with a flat distribution of clusters. The

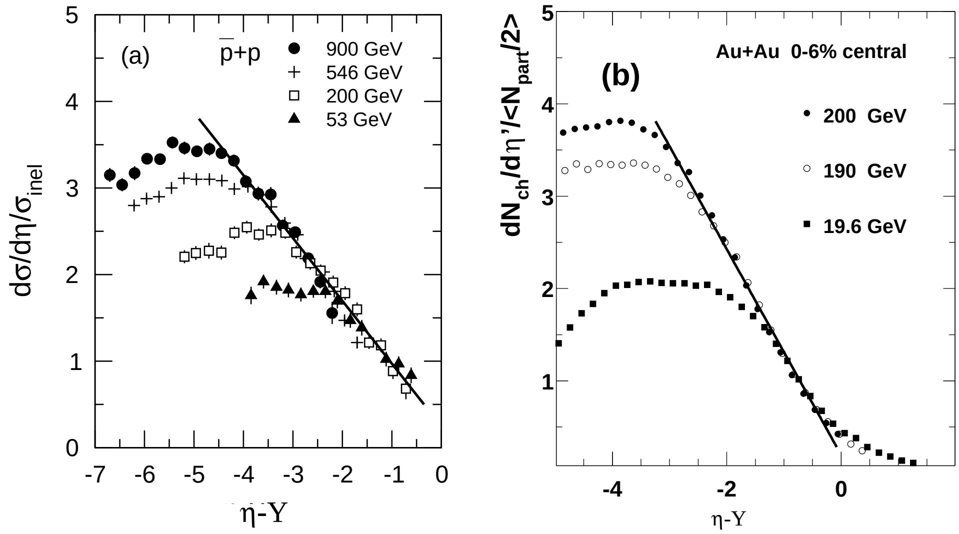

Fig. 1.3. Pseudorapidity distribution for (a) $p\bar{p}$ collisions between $\sqrt{s} = 53$ and 900 GeV [5], (b) AuAu collisions between 19.6 and 200 GeV [11].

saturation in the form of a central plateau then is due to the fact that in the cms only partons can participate with lifetime longer than the time needed for the color exchange.

A remarkable difference is observed between the collider $p\bar{p}$ data [5, 6] and central heavy ion collisions at high energies [13]. In Fig. 1.2(b), $\rho(0)$ is given as a function of $\sqrt{s}$ per participating nucleon pair for both types of collisions. While the lower-energy NA50 point is compatible with the $p\bar{p}$ trend, the higher-energy central heavy ion collisions lead to a $\rho_0(0)$ per participant pair considerably higher than that for $p\bar{p}$ collisions. Therefore, particle production in the former cannot be explained as a simple superposition of nucleon-nucleon interactions.

1.2. Transverse momentum distribution

The differential cross section $d\sigma/dp_{\mathrm{T}}^2$ for positively charged particles (C^+) and for π^- in hp interactions at 250 GeV/c is plotted in Fig. 1.4(a). The data show a significant high-p_{T}^2 tail. Its further increase through ISR, SPS and Tevatron energies [14–16] indicates the onset of a hard-scattering regime. At low p_{T}^2, on the contrary, the exponential slope is largely independent of energy [14–16], and in Fig. 1.4(a), one observes no dependence on the type of beam particle. It is, however, smaller for C^+ than for π^-.

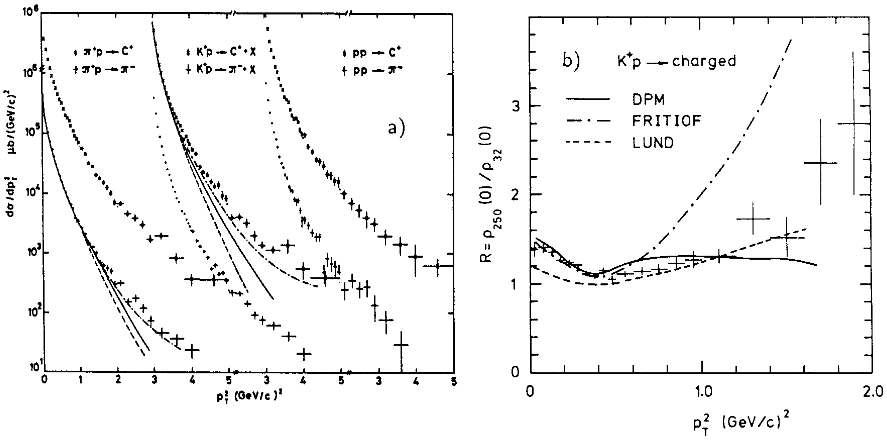

Fig. 1.4. (a) The $d\sigma/dp_{\rm T}^2$ distributions for positively charged particles (C^+) and for π^- in hp interactions at 250 GeV/c. The solid dashed and dashed-dotted curves are DPM, Lund and FRITIOF predictions [1]. (b) The ratio of the central rapidity density *versus* $p_{\rm T}^2$ for K^+p interactions at 250 and 32 GeV/c [1].

The curves in Fig. 1.4(a) reflect the $p_{\rm T}$ parameters used in the particular versions of Lund, DPM and FRITIOF. All models describe the region $p_{\rm T}^2 < 1$ (GeV/c)^2 fairly well, but Lund and DPM clearly do not account for the high $p_{\rm T}^2$ tail of the distributions. Taking into account gluon emission and hard parton scattering processes, FRITIOF describes the inclusive $d\sigma/dp_{\rm T}^2$ distribution better, but still tends to underestimate the data for positive particles in the region $1 < p_{\rm T}^2 < 2.5$ (GeV/c)^2.

In Sect. 1.1 we have analyzed the rise with energy of the central rapidity plateau. Although the effect is well known and also seen in e^+e^- annihilation and deep-inelastic lh processes, the dynamical origin of this phenomenon is not fully understood. In [17] it was shown that part of the central plateau rise is of kinematical origin and related to mass effects which are still significant at top ISR energies. In the framework of the DPM, the effect is purely dynamical and due to *(i)* the increasing overlap in rapidity space of the fragmenting valence-quark chains, *(ii)* the contribution from additional chains stretched between quarks and anti-quarks created in the vacuum. In FRITIOF, the rise of the plateau is a consequence of non-scaling behavior in each string separately, due to gluon emission and the presence of hard scatterings. The latter ingredients are thus expected to reflect in the $p_{\rm T}$-dependence of the plateau rise.

To investigate this question, we plot in Fig. 1.4(b) the ratio of $(d\sigma/dy)_{y=0}$ for charged particles at 32 and 250 GeV/c, as a function of $p_{\rm T}^2$. It is clear that the largest contribution to the total central-plateau increase originates from the *small*-p_{T}^2 region. The ratio is close to one at p_{T}^2=0.5 (GeV/c)^2 and increases again for $p_{\mathrm{T}}^2 > 1$ (GeV/c)^2. A similar energy behavior is observed in ISR data [18]. Furthermore, an additional excess at low p_{T} and at high p_{T} is found when comparing heavy ion collisions to hadron–hadron collisions at the same energy per nucleon [19].

Lund gives $R \approx 1$ around p_{T}^2=0.5 (GeV/c)^2 and $R > 1$ at smaller and larger p_{T}^2, but on both sides R stays smaller than in the data. At least some of this scaling violation derives from the decay of resonances more abundantly produced at larger energies and from kinematics.

FRITIOF, on the other hand, more successful in describing the overall p_{T}^2-spectra, fails to account for the energy dependence in the region $p_{\mathrm{T}}^2 > 0.5$ (GeV/c)^2. The onset of hard parton scatters in this model is so strong between 32 and 250 GeV/c that the prediction overshoots the data by a factor of 1.7 at p_{T}^2=1.0 (GeV/c)^2. DPM describes the rise at small p_{T}^2 reasonably well, but remains almost constant for p_{T}^2 >0.75 (GeV/c)^2. However, for DPM the ratio in this p_{T}^2 region is particularly sensitive to the value of the average primordial quark transverse momentum k_{T}. If the value of $\langle k_{\mathrm{T}}^2 \rangle$ is lowered from 0.42 (GeV/c)^2 to 0.20 (GeV/c)^2, the rise of the ratio for $p_{\mathrm{T}}^2 > 0.75$ GeV/c^2 is similar as in the Lund prediction.

After a first indication in a cosmic ray experiment [20], the UA1 experiment [21] has established an *increase* of the mean transverse momentum $\langle p_{\mathrm{T}} \rangle$ with increasing charged particle density $\Delta n/\Delta y$ in rapidity. A similar increase has been observed in a second cosmic ray experiment [22], in UA5 [23] and at the Tevatron [15]. Though much weaker at ISR energies, an increase is also seen there [18, 24, 25]. Besides the growth of the effect between ISR and Collider, the correlation between $\langle p_{\mathrm{T}} \rangle$ and $\Delta n/\Delta y$ becomes stronger when low p_{T} tracks are excluded and when the analysis is restricted to the central region. Explanations have been proposed in terms of possible evidence for a hadronic phase transition in a thermodynamical model [24, 26, 27], small impact parameter scattering in a geometrical model [28] or the production of mini-jets from semi-hard scattering [29–32].

At lower energies, on the other hand, a *decrease* of $\langle p_{\mathrm{T}} \rangle$ with increasing n had been observed. This decrease is mainly visible at the high-n tail of the distribution and is generally interpreted as a phase-space effect.

Comparing in Fig. 1.5(a) [33] the highest available energy data to intermediate and low energy data, we see that $\langle p_{\mathrm{T}} \rangle$ is surprisingly energy independent for low multiplicities. The slope of $\langle p_{\mathrm{T}} \rangle$ vs. n, on the other hand, is negative for low energies and becomes positive at ISR. This leads to a fast increase of $\langle p_{\mathrm{T}} \rangle$ with increasing energy for high multiplicities. As shown in Fig. 1.5(b), this increase depends on the particle type and is faster for heavier particles than for pions [15].

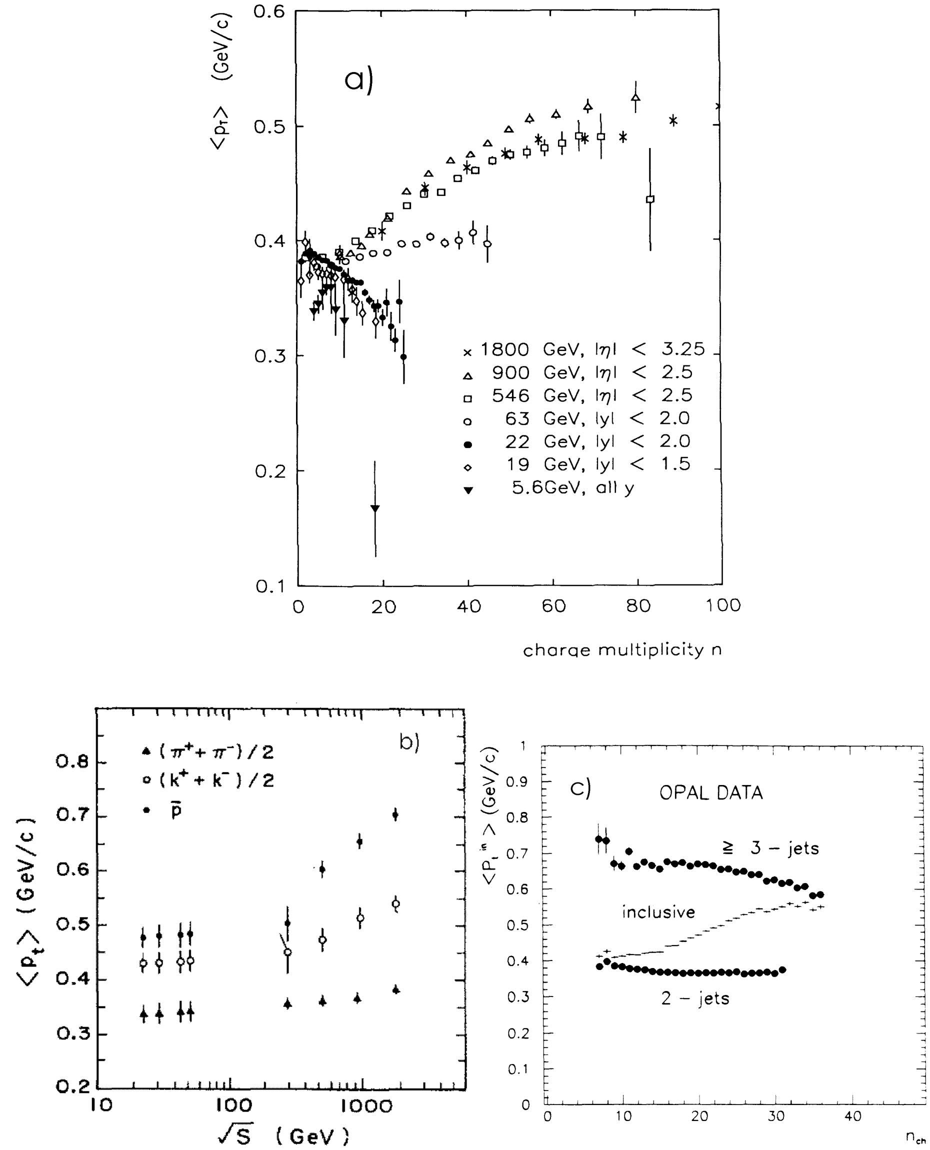

Fig. 1.5. The average transverse momentum $\langle p_\mathrm{T} \rangle$ as a function of charged-particle multiplicity n (a) for hh collisions at $\sqrt{s}$ from 5.6 to 1800 GeV [33], (b) as a function of $\sqrt{s}$ for $\bar{p}$, $\mathrm{K}^{\pm}$ and $\pi^{\pm}$ [15], (c) for inclusive production as well as for 2-jet and $\geq$ 3-jet events in e^+e^- collisions at 91 GeV [34].

The mini-jet interpretation of the development with increasing density and energy in Fig. 1.5(a) gets support from the fact that a similar development is seen in e^+e^- collisions [34, 35]. At 91 GeV, part of the e^+e^- collisions lead to a 2-jet topology, part to a three- or more-jet topology. While the first two jets originate from the fragmentation of the original $q\bar{q}$ pair, the third jet corresponds to a gluon radiated off by one of the quarks. Fig. 1.5(c) shows the average transverse momentum $\langle p_{\mathrm{T}}^{\mathrm{IN}} \rangle$ in the event plane as a function of the charged-particle multiplicity n for inclusive particle production in e^+e^- collisions at 91 GeV [34], compared to that in 2-jet events and ≥3-jet events. While the latter two still show a decrease of $\langle p_{\mathrm{T}}^{\mathrm{IN}} \rangle$ with increasing n, the inclusive distribution shows a clear increase. This increase can be interpreted as due to a change from a 2-jet regime at low n to a ≥3-jet regime at large n [36].

1.3. Differences between quark and gluon jets

The gluon structure function of the proton is considerably softer than the quark ones. UA1 used this difference to perform a statistical separation of quark and gluon jets in two-jet events [37]. In Fig. 1.6(a), the fragmentation function $D(z)$, with the momentum fraction $z = p_z(\text{track})/p(\text{jet})$ and p_z the momentum component along the jet axis, is shown for both types of jets. The ratio of the two distributions is given in Fig. 1.6(b). The softer fragmentation for gluons is indeed also observed in hadronically excited jets, be it with very large errors.

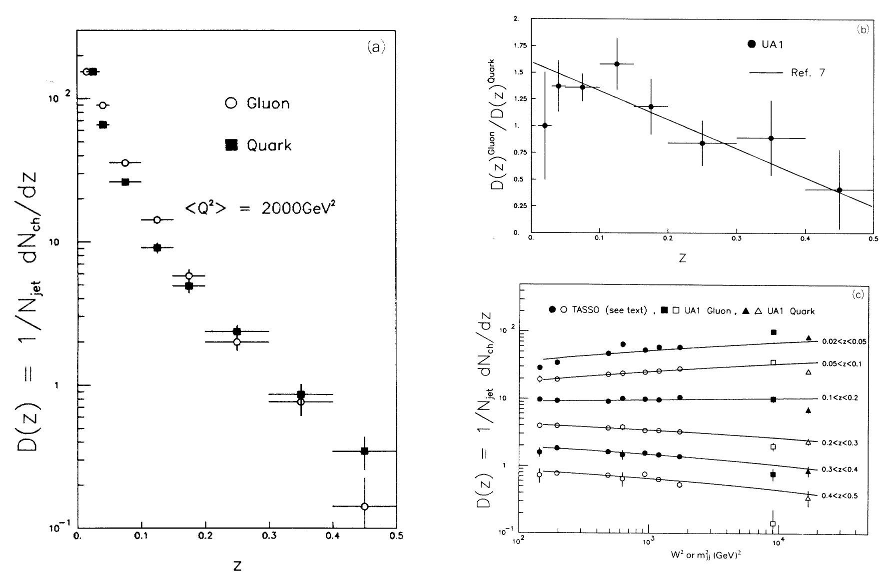

Fig. 1.6. (a) Fragmentation function $D(z)$ for quark jets and gluon jets, (b) their ratio as a function of z. (c) W^2 and m_{jj}^2 evolution of the fragmentation function per bin of z [37].

Furthermore, also here gluon jets are observed to be wider than quark jets, and scaling violations are observed to be stronger than gluon/quark jet differences. In Fig. 1.6(c), the pure quark and gluon fragmentation functions extrapolated from TASSO [38] are given in bins of z versus the two-jet mass, together with UA1 data. In a detailed comparison of the jet shape in e^+e^-, ep and $p\bar{p}$ collisions [39], jets are shown to be narrower in the first two (from OPAL and ZEUS) than in the latter (from CDF and D0). This difference can be understood from the abundance of gluon jets in $p\bar{p}$ collisions at Tevatron energies.

Finally, an analysis of average jet charges demonstrates that gluon jets are neutral, while $u(\bar{u})$-quark-enriched jet samples show a significant positive (negative) average charge.

1.4. The sea gull

A distribution particularly sensitive to the onset of hard effects in lepton-hadron and e^+e^- collisions has turned out to be the energy dependence of the average transverse momentum of particles produced around Feynman-$|x| = 0.4$.

The dependence of the average transverse momentum on Feynman-x has first been observed in hadron–hadron collisions at lower energies [40]. It has a characteristic shape resembling a sea gull with its head lowered at $x = 0$ and its wings raised around $|x| \approx 0.4$. This "sea-gull effect" is also visible in e^+e^- [41] and lh [42, 43] collisions and qualitative similarities between all three types of collisions (hh, lh and e^+e^-) at comparable energies have been observed [43, 44].

In e^+e^- annihilation, a dramatic rise with cms energy [41] has set in for one of the wings, as a consequence of the onset of emission of a hard gluon by one of the two leading quarks. This rise is satisfactorily reproduced by a QCD model of independent quark fragmentation [45] and by a string model [46] when hard processes are included. For e^+e^- annihilation, these processes become significant at an energy of about 10 GeV and lead to a rise of $\langle p_\mathrm{T}^2 \rangle$ by a factor of two from 14 to 22 GeV.

Neutrino experiments [42] have shown that already at hadronic masses $W < 10$ GeV, the sea gull is lifting its current-fragmentation wing with increasing W. The EMC collaboration [43] has increased the W range up to 20 GeV and shown that in terms of Lund fragmentation, this effect can be reproduced only if gluon radiation is included.

The point is, that a rise of the sea-gull wings is also observed in hadron–hadron collisions at comparable energy. As in lepton-hadron collisions, the rise may have set in at lower energies [47, 48], but is clearly visible in K^+p collisions from 12.7 to 250 GeV/c ($\sqrt{s} \approx$ 5–22 GeV) in Fig. 1.7(a) [49].

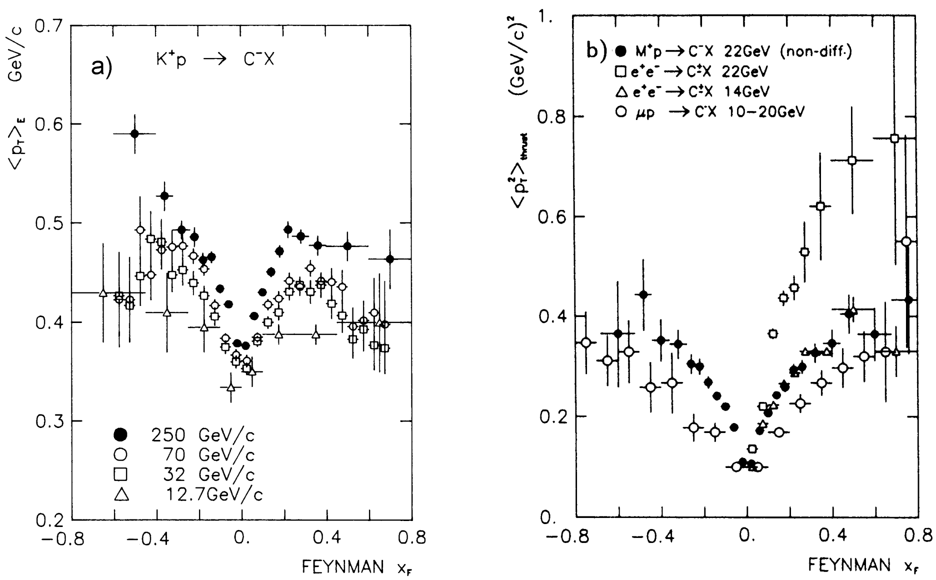

Fig. 1.7. (a) The energy weighted average transverse momentum $\langle p_{\mathrm{T}} \rangle_E$ as a function of Feynman-x for $K^+p \rightarrow C^- + X$ between 12.7 and 250 GeV/c incident momentum. (b) The average squared transverse momentum $\langle p_{\mathrm{T}}^2 \rangle_{\mathrm{thrust}}$ with respect to the thrust axis for the combined non-single-diffractive K^+p and π^+p sample (indicated as M^+p) with multiplicity $n \geq 4$ at $\sqrt{s} = 22$ GeV, compared to that for e^+e^- collisions at 14 and 22 GeV, and μp collisions with $10 < W < 20$ GeV [49].

In Fig. 1.7(b), the combined non-single-diffractive K^+p and π^+p data are compared to e^+e^- results at $\sqrt{s} = 22$ and 14 GeV and to μp results at $10 < W < 20$ GeV in terms of $\langle p_{\mathrm{T}}^2 \rangle_{\mathrm{thrust}}$, the average of the square of the particle p_{T} with respect to the thrust axis. In the hh data, the wings of the sea-gull distribution are significantly lower than the (folded) wings from e^+e^- at the same energy, but higher than those from μp collisions with hadronic energy $10 < W < 20$ GeV. The meson fragmentation wing at 22 GeV is consistent with the folded e^+e^- wings at 14 GeV.

From Figs. 1.7(a) and b we, therefore, conclude that a rise of the sea-gull wings with cms energy is also observed for hh collisions, but the rise is less dramatic than in e^+e^- annihilation. Part of this difference can be explained by heavy quark fragmentation contributing in e^+e^-, but not in hh collisions. Furthermore, the hadronic energy ($\sqrt{s}$ or W) has to be shared by more quarks in lh and hh collisions than in e^+e^- collisions.

1.5. Resonances

About 50% of the pions shown in Fig. 1.1 come from vector mesons and also tensor mesons and baryon resonances are not negligible as pion sources. So, more direct information on the production mechanism can be expected from the study of resonances.

1.5.1. Total yields and strangeness suppression

A systematic study of particle and resonance yields has been performed [50] with pp interactions at $\sqrt{s} = 52.5$ GeV. As can be seen in Fig. 1.8, the particle yield falls exponentially with particle mass, but separately for strange and non-strange mesons. The line connecting the strange mesons lies about a factor $1/\lambda \approx 3$ lower than that for the non-strange ones. An important exception is the ϕ meson, which is an $s\bar{s}$ quark state. This lies considerably *below* the strange-meson line, in agreement with a double strangeness suppression λ^2.

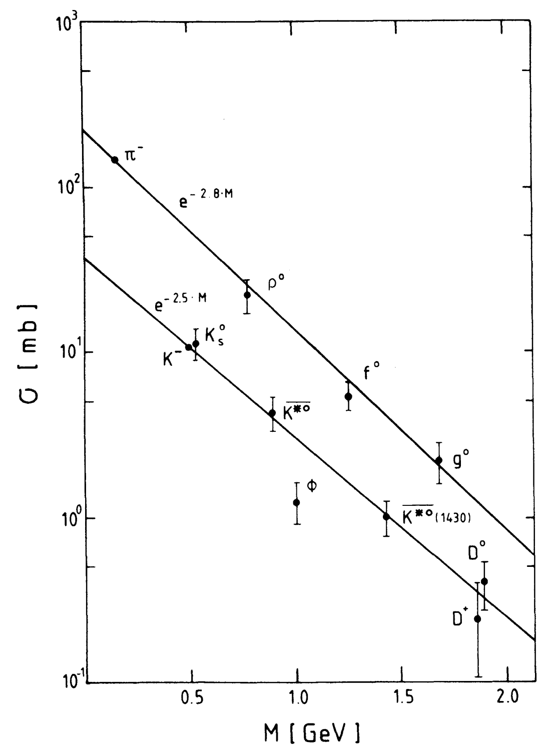

Fig. 1.8. Resonance cross section from pp collisions at $\sqrt{s} = 52.5$ GeV as a function of the resonance mass [50].

The strangeness suppression factor has been measured at several energies. There is an indication of an s dependence at small s, but the data are compatible for hadron–hadron, e^+e^- and lepton–hadron data with $\lambda = 0.295 \pm 0.006$ as the most accurate estimate [51].

It does, however, depend on the region of phase space studied [52, 53]. For example, as determined by the ratio $\sigma(\phi)/\sigma(K^*_{892})$ in NA22, λ decreases with increasing Feynman-x and drops to $\lambda \approx 0.1$ near $x = 1$.

1.5.2. Feynman-x and rapidity dependence

Of particular importance in particle or resonance production is their Feynman-x dependence. The yield of particles and resonances differs strongly for different x regions, and the consequent x dependence depends strongly on the quantum numbers of the beam and the produced particle.

A good demonstration for the existence of a quantum number dependence of resonance production is the difference between positive and negative $\Sigma(1385)$ from K^-p collisions studied at 4.2, 10, 14.3 and 16 GeV/c beam momentum [54–56]. The $\Sigma^-(1385)$ is produced symmetrically with respect to $x = 0$, with vanishing cross section for x near unity (see Fig. 1.9 for 10 GeV/c). The $\Sigma^+(1385)$ has a large cross section for all $x < 0$, but is about equal to $\Sigma^-(1385)$ for $x > 0$. In the proton fragmentation region Σ^- production should be small, as it requires double charge exchange, whereas Σ^+ is allowed. The difference shown in Fig. 1.9 then suggests a fragmentation component, the equal part a central component.

The rapidity distribution for $\rho^{\pm 0}$ (Fig. 1.10(b)) produced from pp at 24 GeV/c [57] is in qualitative agreement with that of $\Sigma^-(1385)$ in K^-p reactions and thus suggestive of being due to largely central production. It is interesting to note that the distributions for ρ^+, ρ^- and ρ^0 are the same.

For $\rho^{\pm 0}$ produced from π^+p at 16 GeV/c as shown in Fig. 1.10(a), equality of the rapidity distribution holds only for $y < 0$. For $y > 0$, only ρ^- is approximately symmetric to the negative y region. The cross section for ρ^+ and ρ^0 stays large for all $y > 0$ and about twice as large for ρ^+ as for ρ^- in the beam fragmentation region. This is again in agreement with suppression of ρ^- in the π^+ fragmentation region due to double charge exchange.

In Fig. 1.10(c), the rapidity density $(1/\sigma_{\rm inel})(d\sigma/dy)$ is compared for ρ^- produced from pp (circles) and π^+p (crosses). In the whole y region, the distributions are quite similar, in agreement with the expectation of dominant central production in both experiments. As can be deduced from Figs. 1.10(a) and (b), this equality also holds for ρ^+ and ρ^0 production for $y < 0$ where central production is expected to dominate. As expected for a fragmentation component, for $y > 0$ the ρ^0 and ρ^+ production becomes significantly larger in the π^+p than in the pp reactions.

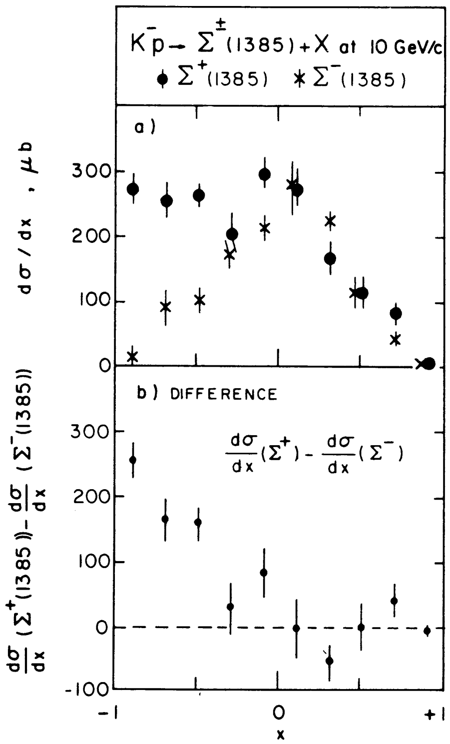

Fig. 1.9. (a) Differential cross section $d\sigma/dx$ for $\Sigma^+(1385)$ and $\Sigma^-(1385)$ inclusive production at 10 GeV$/c$. (b) Difference between the $d\sigma/dx$ distribution for $\Sigma^+(1395)$ and that for $\Sigma^-(1385)$ [56].

We conclude from this that, in spite of the failure of central boost invariance observed in Sect. 1.1, there is good evidence for a two-component picture of inclusive particle and resonance production, already at rather low energy. The fragmentation component depends on the produced particle or resonance and on the fragmenting incoming particle. The shape of the central component is universal, *i.e.*, does neither depend on the incoming particles nor on the produced particle or resonance.

Furthermore, it has been noted that only of the order of 10% of the pions are produced directly (the largest pion sources being $\rho^{\pm 0}$ and ω^0) and that strangeness is suppressed by a factor $1/\lambda \approx 3$.

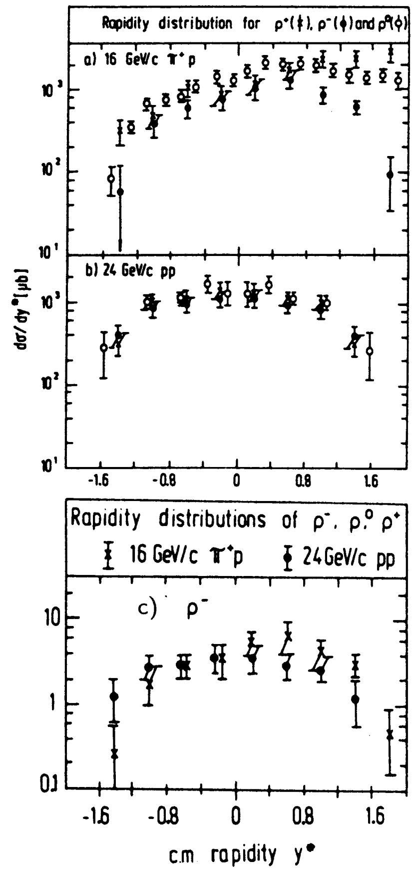

Fig. 1.10. Differential cross section $d\sigma/dy$ for inclusive $\rho^{\pm 0}$ production as a function of y in (a) π^+p reactions at 16 GeV/c, (b) pp reactions at 24 GeV/c. (c) Comparison of the inclusive ρ^- density in 16 GeV/c π^+p and 24 GeV/c pp interactions [57].

1.6. Reflection of the valence quark distribution

The antiquark distribution in the proton is concentrated at small Bjorken-$x_{\rm B}$ (say, $x_{\rm B} \leq 0.2$, the sea region) and the same is true for gluons which dissociate into a $q\bar{q}$. The presence of an $\bar{q}$ component in the proton structure function implies that the proton, which primarily consists of three quarks, is subject to fluctuations in which extra $q\bar{q}$ pairs are formed. According to the suggestion of Ochs [58], proton fragmentation in the collision with other hadrons may then be viewed as a rearrangement of the pre-existing partons preserving approximately their individual longitudinal momenta.

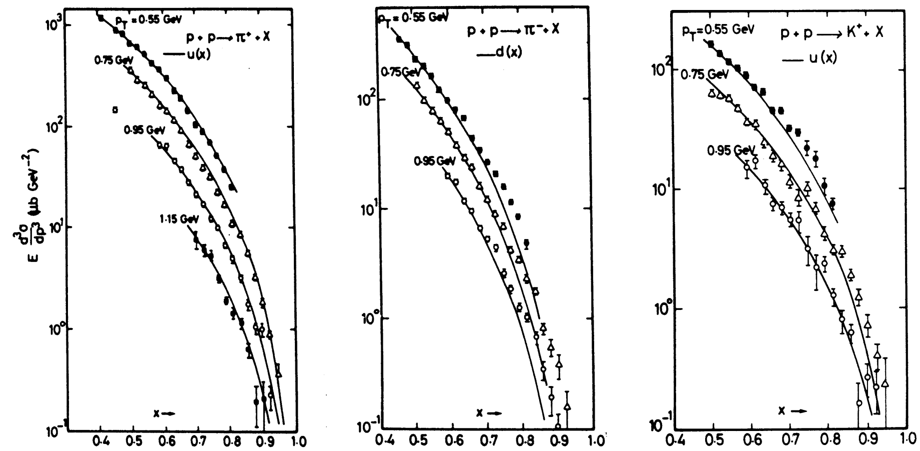

Fig. 1.11. Comparison of the invariant π^+, π^- and K^+ cross section as a function of Feynman x from pp collisions at $\sqrt{s} = 45$ GeV to the u- and d-quark distribution functions $u(x_{\rm B})$ and $d(x_{\rm B})$, respectively [59].

In the fragmentation region of the proton, the π^+ can be assumed to be composed of a u valence and a $\bar{d}$ sea quark. Since the latter carries very little momentum, we expect to find a $\pi^+ = |u\bar{d}\rangle$ with momentum similar to that of the u quark. The same holds for a $\pi^- = |d\bar{u}\rangle$ and the d quark. As a consequence, the Feynman-x distribution of a pion in the fragmentation region of an incident proton is expected to be similar to the $x_{\rm B}$ distribution of the valence quark which it shares with the proton. Fig. 1.11(a) shows [59] that the x distribution of the π^+ produced in pp collisions at ISR is indeed similar to the proton u-quark distribution $u(x_{\rm B}) \equiv F_u^p(x_{\rm B})$ derived from electron–nucleon deep inelastic scattering. The π^- distribution (Fig. 1.11(b)) agrees with the proton d-quark distribution $d(x_{\rm B}) \equiv F_d^p(x_{\rm B})$ up to $x_{\rm B} \approx 0.7$, and is only slightly above $d(x_{\rm B})$ for larger $x_{\rm B}$ values.

Furthermore, the K^+ distribution agrees again with $u(x_{\rm B})$, as expected from the fact that it shares a u quark with the proton (Fig. 1.11(c)). The K^- has no valence quark in common with the target proton. Indeed, its x distribution (not shown) falls much more steeply with increasing x than either $u(x_{\rm B})$ or $d(x_{\rm B})$.

We conclude that the quantum numbers and the momentum distribution of the target–proton valence quarks can be found back in the particles produced in the target fragmentation region.

1.7. Conclusions

Within hadron–hadron collisions, meson ($\pi^{\pm}$, $K^{\pm}$)-proton collisions have the advantage of being a simple $q_1\bar{q}_2$ system and representing a large flavor variety. Quite surprisingly, this quark flavor is observed to play an essential role in these (soft!) collisions and its fragmentation is found to be similar to the fragmentation of the corresponding quark in e^+e^- collisions and DIS. Furthermore, the quantum numbers and momentum distribution of the target-proton valence quarks can be found back in the particles produced in the target fragmentation region. On the other hand, hadron production in the central region (near zero rapidity) is independent of the quantum numbers of beam or target.

The disadvantage is that meson beams only exist up to 250 GeV lab momentum ($\sqrt{s} = 22$ GeV), so that they have to be complemented by $p^{\pm}p$ collisions at higher energies, for other important features, as scaling violation in the central region or p_{T} evolution with increasing energy and particle multiplicity.

The fact that jets produced along the beam direction in ordinary hadron–hadron collisions are similar to those produced in e^+e^- annihilation and deep inelastic leptoproduction has led to the assumption of parton fragmentation as a common underlying dynamical mechanism.

2. Final-state multiplicity

2.1. Average multiplicity and its energy dependence

The average number of particles, of all types or of a particular type, is the first moment of the multiplicity distribution and the phase-space integral of the corresponding singe-particle density. As such, it does not contain any information on correlations, but is one of the basic observables characterizing hadronic final states and their evolution with increasing energy.

An early question was how the average multiplicity and its energy evolution depend on the type of collision. The average multiplicity $\langle n\rangle$ of charged hadrons produced in $\bar{\nu}p$ collisions is plotted in Fig. 2.1(a) as a function of the squared hadronic energy W^2 for $W^2 < 100$ GeV [61]. One can discuss the small systematic differences between the three experiments shown, but one cannot deny the success of the fit represented by the full line. However, the fit is not to these $\bar{\nu}p$ data, but to non-diffractive π^-p data at corresponding cms energy [60]! So, one observes the relation $\langle n\rangle_{\bar{\nu}p} = \langle n\rangle_{\pi^-p}$.

Similarly, $\langle n\rangle$ is given as a function of the cms energy $\sqrt{s}$ for early e^+e^- annihilation [62] results in Fig. 2.1(b). Since no proton fragmentation is involved in e^+e^- and protons fragment differently, proton fragmentation has to be removed from the hadronic counterpart, here. This can be done

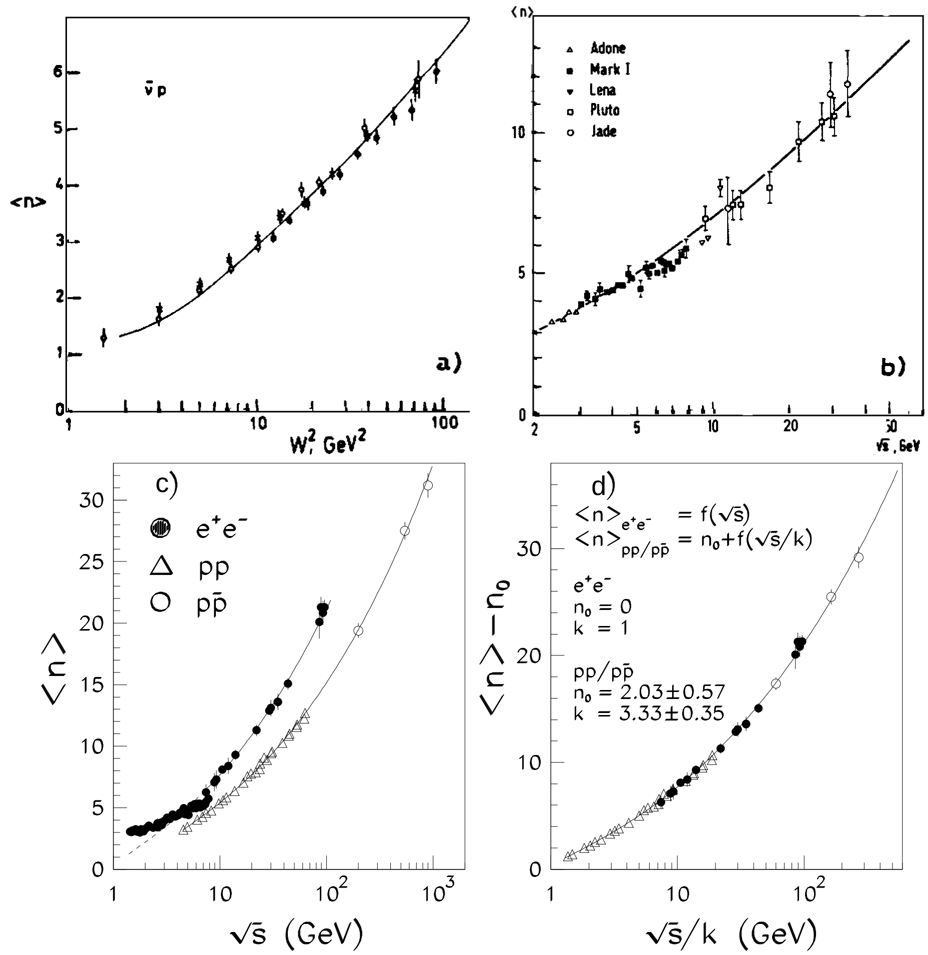

Fig. 2.1. Average charged-particle multiplicity of the hadronic system in (a) $\bar{\nu}p$ collisions [61] (the solid line shows a fit [60] to the non-diffractive component of π^-p collisions), (b) e^+e^- annihilation [62] (the solid line shows the prediction from hadronic data according to (2)); (c) e^+e^- compared to $pp^\pm$ collisions [63]; (d) comparison after the transformation $\langle n\rangle \to \langle n\rangle - n_0$, $\sqrt{s} \to \sqrt{s}/k$ for $pp^\pm$ collisions [63].

by using

$$\langle n\rangle_{e^+e^-} = \langle n\rangle_{\pi^+p} + \langle n\rangle_{\pi^-p} - \langle n\rangle_{pp}\,. \tag{2}$$

Indeed, a fit through the right-hand-side combination of non-diffractive hadronic multiplicities [60] reproduces the e^+e^- data for $\sqrt{s} < 50$ GeV.

In the meantime we have moved to higher energies, in particular with e^+e^- and $p\bar{p}$ collisions, but not with π^-p collisions. So, other comparisons have been made.

Of course, it is evident that the simple similarities observed above cannot persist. Besides the absence of proton fragmentation in e^+e^- collisions mentioned above, *e.g.*, hard gluon radiation leads to 3- and 4-jet events in e^+e^- collisions, while hard parton scattering leads to 4-jet events in hh collisions. Both mechanisms cause an increase in the number of particles produced, but the relative strength of these two mechanism is different in the two types of collisions.

Nevertheless, Fig. 2.1(c) gives a comparison [63] of e^+e^- and $pp^\pm$ collisions at higher energies. In both cases, the energy dependence of $\langle n\rangle$ can be well described by [64]

$$\langle n\rangle \;=\; a_0 + a_1 \exp\left(a_2\sqrt{\ln s}\right) , \tag{3}$$

or

$$\langle n\rangle \;=\; c_0 + c_1 \ln s + c_2(\ln s)^2 , \tag{4}$$

but at given energy, $\langle n\rangle$ is about 25% lower for $pp^\pm$ collisions than for e^+e^- annihilation.

Following an earlier comparison [65], in Fig. 2.1(d) [63], the average $pp^\pm$ inelasticity and leading system fragmentation have been taken into account by the transformation $\langle n\rangle \to \langle n\rangle - n_0$, $\sqrt{s} \to \sqrt{s}/k$, with n_0 and k as additional fit parameters for the $pp^\pm$ data. Both parametrizations (3) and (4) give excellent combined fits, with similar n_0 and k values. The latter suggest that together the leading $pp^\pm$ systems on average contribute about 2 charged particles, while the energy available to central particle production is about 1/3 of the total energy.

2.2. The shape of the multiplicity distribution and its energy dependence

The shape of the multiplicity distribution P_n, and in particular its deviation from a Poissonian, gives the amount of correlation in the production of final-state particles. Positive correlations lead to a distribution wider than Poisson, negative correlations to a distribution narrower than Poisson.

Examples are shown in Fig. 2.2 in terms of the so-called KNO (Koba–Nielsen–Olesen) form [66],

$$\psi(z) \equiv \langle n\rangle P_n \tag{5}$$

as a function of $z = n/\langle n\rangle$, for $pp^\pm$ [67] and for e^+e^- collisions [68]. While $pp^\pm$ collisions lead to a wide distribution, widening with increasing energy, e^+e^- collisions lead to a relatively narrow distribution with only little energy dependence.

To arrive at more quantitative statements, the shape can be fitted by an analytical form parametrizing the multiplicity distribution in terms of two

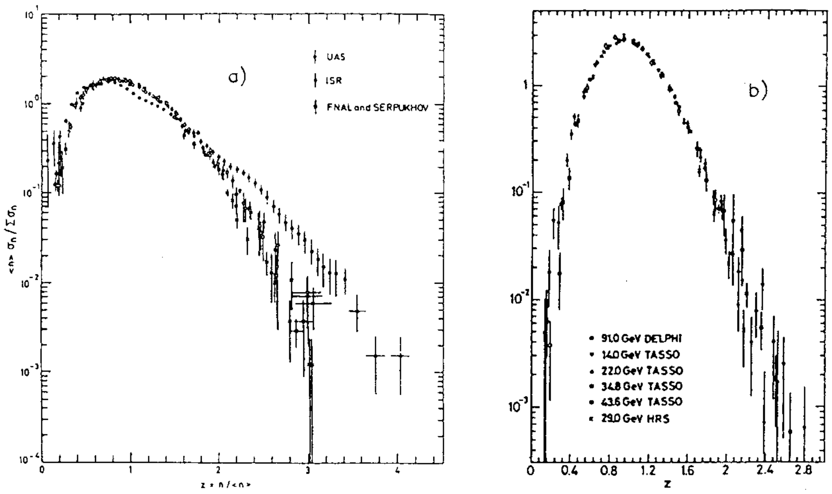

Fig. 2.2. The shape of the multiplicity distribution in KNO form for (a) $pp^{\pm}$ collisions [67], (b) $e^{+}e^{-}$ collisions [68].

or more free parameters or, alternatively, it can be studied in terms of its moments of rank $q \geq 2$.

One of the most striking phenomena emerging from studies of multiplicity distributions is the wide occurrence of the negative-binomial distribution

$$P_n(\bar{n}, k) = \frac{1}{n!}\frac{\Gamma(k+n)}{\Gamma(k)}\left(\frac{\bar{n}}{k}\right)^n\left(1+\frac{\bar{n}}{k}\right)^{-n-k} \quad . \tag{6}$$

For the two independent parameters, one usually chooses the average multiplicity[1] $\bar{n}$ and a parameter k describing the shape of the distribution. The dispersion D is given by

$$\left(\frac{D}{\bar{n}}\right)^2 = C_2 - 1 = \frac{1}{\bar{n}} + \frac{1}{k}\,. \tag{7}$$

From (6), the negative binomial is wider than Poisson as long as k is positive and finite. In the limit $k \to \infty$ the negative binomial reduces to the Poisson distribution

$$P_n = e^{-\bar{n}}\frac{\bar{n}^n}{n!}\,. \tag{8}$$

[1] We denote by $\bar{n}$ the average over the distribution as distinct from $\langle n \rangle$, the average over the experimental sample.

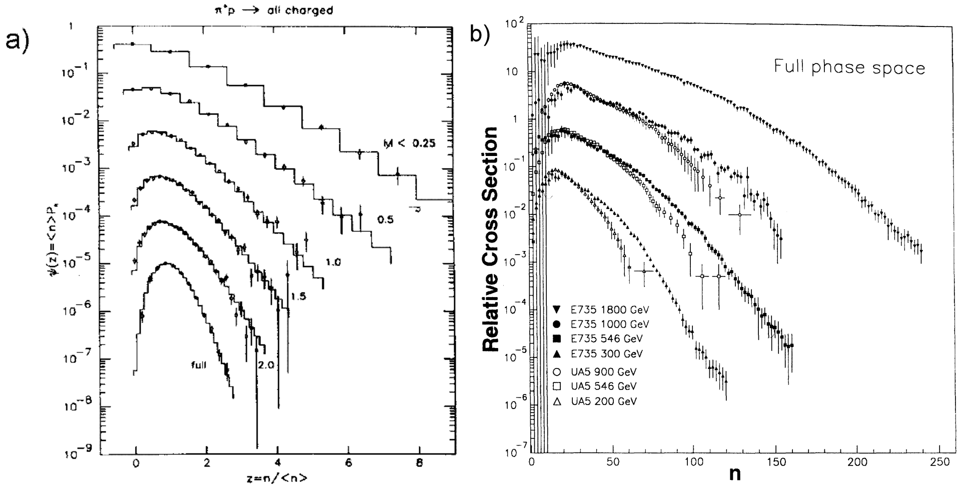

Fig. 2.3. (a) Charged-particle multiplicity distribution for non-single diffractive π^+p data $\sqrt{s} = 22$ GeV in different rapidity intervals $|y| < y_{\rm cut}$ and full phase space, in KNO form, together with the best-fit negative binomials [73]; (b) Charged-particle multiplicity distribution for non-single-diffractive $p\bar{p}$ data as measured by UA5 and E735 at various collider energies. Data from the two experiments at the corresponding energy are normalized to each other over a range of n just past the peak of the distribution [79].

If k is a negative integer, the negative binomial becomes a (positive) binomial distribution, which is narrower than Poisson.

The usefulness of the negative-binomial distribution in describing full-phase-space multiplicity distributions was already shown in the early seventies [69]. However, the interest was revived by the observation of the UA5 collaboration [70] that the charged-particle multiplicity of non-diffractive pp and $p\bar{p}$ collisions is well described by the even component of a negative-binomial distribution, from a center of mass energy $\sqrt{s}=10$ to $\sqrt{s}=546$ GeV.

Moreover, the same collaboration found for non-diffractive $p\bar{p}$ collisions at $\sqrt{s} = 546$ GeV, that not only the full-phase-space multiplicity distribution appears to be of this type, but also the distribution within central pseudo-rapidity intervals [71]. Since then, negative binomials have been successfully fitted to multiplicity distributions in full and in limited phase space for hh, hA and AA collisions at other energies [63, 72–82], as well as for lh [83–85] and e^+e^- collisions [86–90]. An example is given in Fig. 2.3(a).

Based on these findings, a large number of possible physical interpretations have been given for negative-binomial or negative-binomial-like distributions. Summaries can be found in [91]. In general, the interpretations can be classified [92] as being of (partial) stimulated emission or of cascading type. A number of critical comments on the applicability of negative binomials in full phase space, mainly based on the influence of the conservation laws, can be found in [93].

At the highest energies of $\sqrt{s} = 900$ GeV [78] and 1800 GeV [79, 81], a shoulder is building up at high n (Fig. 2.3(b)), so that the distribution can not be fitted by a single negative binomial any more. This is interpreted in terms of the presence of two components, one corresponding to conventional soft physics, the other to QCD semi-hard mini-jets [94], one to a pure birth, the other to a Poisson process [95] or, alternatively, to multiparton collisions and multichain production [79, 96].

Another approach [97] is to understand particle production as a two-cascade process, where the first cascade is responsible for the partons or strings, the second for their fragmentation into hadrons. The composition of two Poisson distributions, each describing one of these two Markov type branching processes, can lead to oscillations in P_n at the upper SPS and Tevatron energies.

A similar structure, though less pronounced, is becoming visible in e^+e^- collisions at the Z^0 [88], but is not observed in DIS [85] so far.

Koba, Nielson and Olesen [66] have shown that, if Feynman scaling [4] holds, the function $\psi(z)$ of (5) becomes asymptotically ($n \to \infty, \langle n \rangle \to \infty$, z fixed) independent of $\sqrt{s}$. Note that (5) corresponds to rescaling the P_n curves corresponding to the collision energy by stretching the vertical axis and shrinking the horizontal axis both by $\langle n(s) \rangle$, thus maintaining normalization. If $\psi(z)$ is independent of $\sqrt{s}$ then also its normalized moments $C_q = \langle n^q \rangle / \langle n \rangle^q = \int_0^\infty z^q \psi(z) dz$ or its normalized factorial moments F_q (*e.g.* $F_2 = C_2 - 1/\langle n \rangle$).

Even though the original derivation from Feynman scaling turned out to be wrong [98], Feynman scaling is known to be violated (see Sect. 1.1), and the increase of $\langle n \rangle$ with s faster than logarithmic in Fig. 2.1, KNO scaling is often claimed for full-phase-space and single-hemisphere multiplicity distributions in e^+e^-, lepton–hadron and medium energy (ISR) hadron–hadron collisions [93, 99]. It was demonstrated [100] even earlier, however, that KNO scaling should hold approximately more generally in any model based on a scale-invariant stochastic branching process with an energy-independent coupling constant.

With high-energy (SPS and Tevatron) $p\bar{p}$ collisions, UA5 [67, 72, 78, 101] and E735 [79] and to some extent also UA1 [102] could show that the scaling at ISR energies was accidental and that KNO scaling is in fact violated in hh collisions up to at least 2 TeV (see Fig. 2.4(a) for the energy dependence of the C_q moments up to 0.9 TeV).

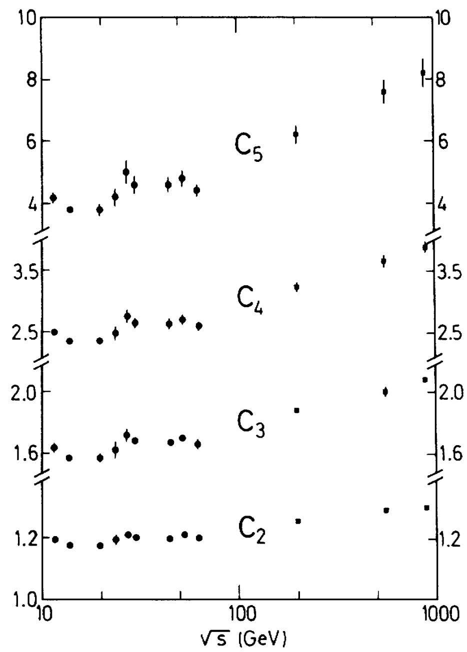

Fig. 2.4. The energy variation of the C-moments of the charged-particle multiplicity distribution for non-single diffractive $pp^{\pm}$ collisions [78].

In connection with the negative binomial it is important to note that, according to Feynman scaling, it should be the factorial moments

$$F_q \equiv \langle n(n-1)\ldots(n-q+1)\rangle/\langle n\rangle^q = k(k+1)\ldots(k+q-1)/k^q \qquad (9)$$

which are expected to be constant [103], and the reduced moments C_q (used by KNO) only in the approximation $\langle n\rangle \approx \bar{n} \gg q$. In fact, from Eq. (7), a constant $\langle n\rangle/D$ at non-zero $1/\langle n\rangle$ would require an *increasing* $1/k$, in particular up to the LEP energy range! Furthermore, contrary to the C_q, the F_q and k tend to finite limits as $\bar{n} \to 0$ and therefore provide a better measure of the shape of a multiplicity distribution at small $\bar{n}$.

In Fig. 2.5, a compilation [104] of the parameter $1/k$ is given as a function of $\ln\sqrt{s}$ for hh, lh and e^+e^- collisions. At given $\sqrt{s}$, the value of $1/k$ is lower for e^+e^- and lh than for hh collisions. However, in all cases, $1/k$ increases with increasing energy from a negative value at low energies to a positive one above a certain Poisson-like ($1/k = 0$) transition point. The transition point is at $\sqrt{s} \approx 5$ GeV for hh and $\sqrt{s} \approx 20 - 30$ GeV for e^+e^- collisions, but the increase is quite similar up to about 50 GeV. At LEP energies, $1/k$ tends to flatten for e^+e^- collisions [88–90]. So, contrary to hh collisions,

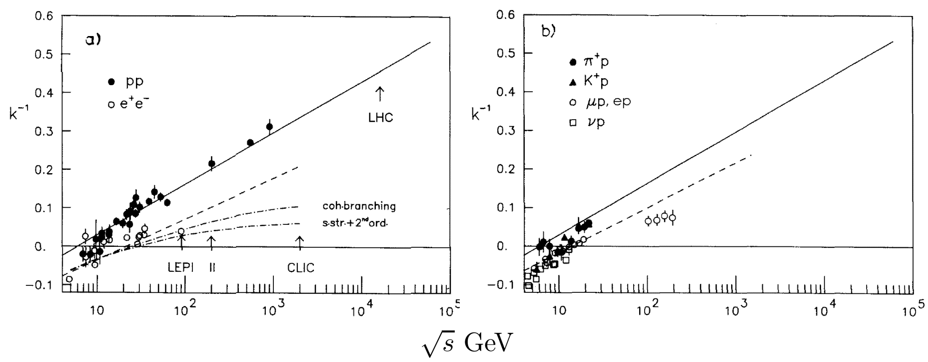

Fig. 2.5. (a) Negative-binomial parameter 1/k for non-single diffractive $pp^{\pm}$ collisions and for e^+e^- annihilation as a function of $\ln\sqrt{s}$. The full line is a linear fit to the $pp^{\pm}$ data, the dashed line to the e^+e^- data below 50 GeV. The dash–dot lines correspond to the predictions from coherent gluon branching and single-string plus second order corrections in JETSET, as indicated. (b) Negative-binomial parameter $1/k$ for non-diffractive π^+p collisions and for lh collisions as a function of $\ln\sqrt{s}$. The full line is the linear fit to the $pp^{\pm}$ data of sub-figure (a). The dashed line is a fit to the μp data (below 50 GeV) [104].

an approach to KNO scaling may be observed for e^+e^- collisions. It is important to note, however, that the flattening takes place at a positive $1/k$ value. So, the distribution is wider than Poisson, even for e^+e^- collisions.

The increase of $1/k$ for e^+e^- collisions up to 45 GeV and flattening above that is reproduced by both the JETSET [105] (Fig. 2.5) and HERWIG [106] models. At higher energies more than 2nd order corrections are needed but coherent branching predicts negative-binomial-like multiplicity distributions up to the highest energies ($\sqrt{s} = 2$ TeV) [107]. Above $\sqrt{s} \approx 25$ GeV these are wider than Poisson ($1/k > 0$).

The KNO form (5) can be generalized [108] as

$$P(n, s) = \frac{1}{\lambda(s)}\psi\left(\frac{n + c(s)}{\lambda(s)}\right), \tag{10}$$

with an energy-dependent scale parameter $\lambda(s)$ corresponding to $\langle n\rangle$ and an energy-dependent location parameter $c(s)$, associated with leading particle effects. Even though there is no experimental evidence for an energy-dependent shift at very high energies (*i.e.* $c(s) = 0$), this form has led [109] to the alternative ansatz

$$P(\ln n, s) = \frac{1}{\lambda(s)}\varphi\left(\frac{\ln n + c(s)}{\lambda(s)}\right). \tag{11}$$

This ansatz is based on Polyakov's original self-similar, scale-invariant branching model interpretation [100] leading to the negative-binomial type scaling

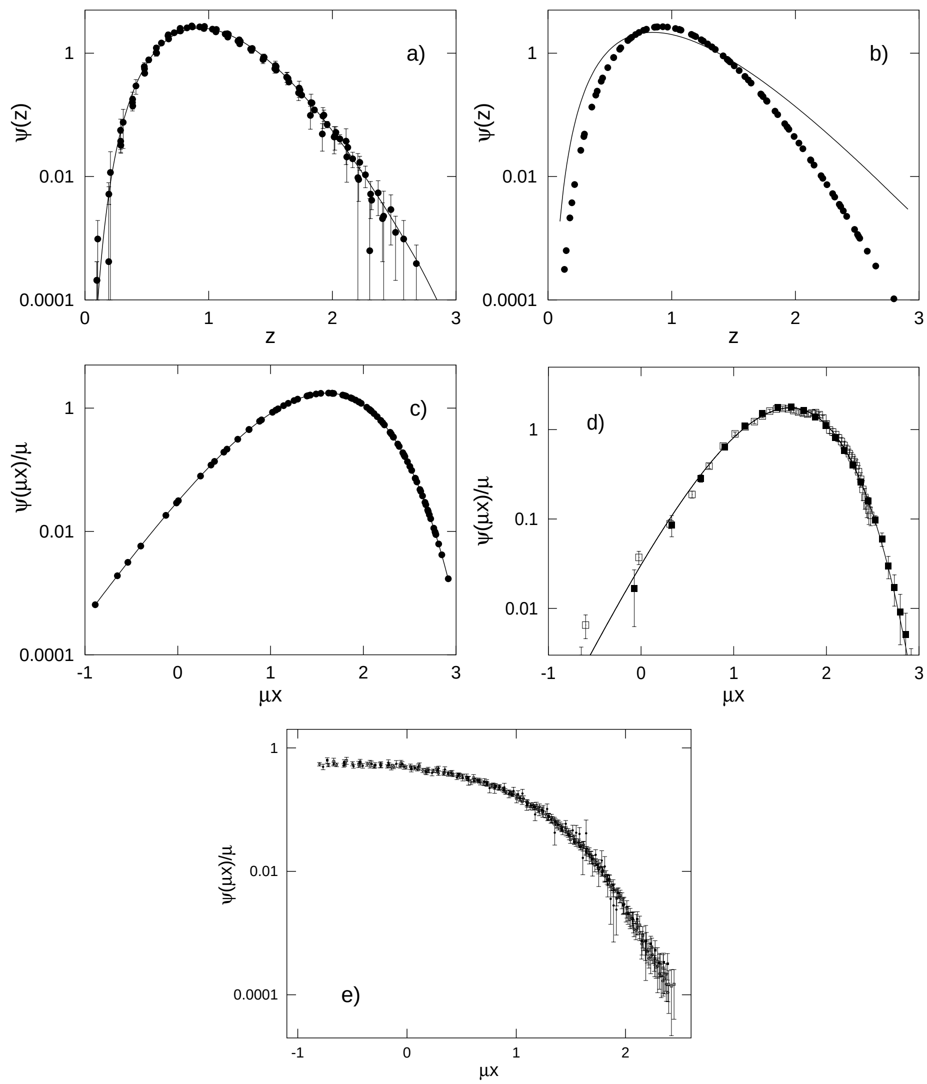

Fig. 2.6. The LEPI data [88–90, 111] for the full-phase-space multiplicity distributions (dots) compared to Eq. (13) with $k = 5$ and $\mu = 5/3$ (solid line). (b) $\psi(z)$ with $\mu = 5/3$ (dots) evolves to $\psi(z)$ with $\mu = 1$ (solid line) at $s \to \infty$. (c) The scaling behavior is recovered in $\psi(\mu x)/\mu$ versus μx. (d) Comparison of the UA5 non-diffractive data at $\sqrt{s} = 546$ GeV [78] and the OPAL data at $\sqrt{s} = 91.2$ GeV [89]. The solid curve is (14) with $k = 5$. (e) Log-KNO scaling of the E735 data [79, 109].

function (gamma distribution in z^μ, *i.e.* the rescaled multiplicity to the power μ)

$$\psi(z) \propto a(z)\exp(-z^\mu)\,, \quad \mu > 1\,, \tag{12}$$

with $a(z)$ being a monomial in z. In the language of QCD, taking into account higher-order effects responsible for energy-momentum conservation in parton jets [110], this reads

$$\psi(z) = \frac{\mu D^{\mu k}}{\Gamma(k)} z^{\mu k-1}\exp(-[Dz]^\mu)\,, \tag{13}$$

with $k = 3/2$, $\mu = (1-\gamma_0)^{-1}$ and D being a γ_0 dependent scale parameter.

Obviously, this distribution shows KNO scaling (s-invariance) for fixed coupling. On the contrary, violation of KNO scaling is expected from the running of $\alpha_{\rm s}(s)$ in the form of a tail of $\psi(z)$ widening with increasing s (Fig. 2.6(a) and (b)).

Rewriting the Polyakov–Dokshitzer form (13) as

$$\psi(x) = \frac{\mu}{\Gamma(k)}\exp(k\mu x - e^{\mu x})\,, \quad x = \ln(Dz)\,, \tag{14}$$

the multiplicity scaling violated by QCD effects is recovered by plotting $\mu^{-1}\psi(\mu x)$ as a function of μx, *i.e.* by a location and scale change of $P(\ln n, s)$ governed by the QCD anomalous dimension (Fig. 2.6(c)). This property is referred to as log-KNO scaling [109].

It comes as a surprise that even the non-diffractive $p\bar{p}$ collisions [78] fall onto the e^+e^- curve (see Fig. 2.6(d)).

Restricting oneself to n values above the shoulder observed in the E735 data in Fig. 2.3(b), log-KNO scaling is observed also there, but the scaling function looks different ($k = 1/2$, μ decreasing from 2.2 to 1.7 between 300 and 1800 GeV). Note that scaling is observed within the two $p\bar{p}$ experiments, but not between the two. This difference, already visible in Fig. 2.3(b), is a severe experimental problem, which will have to be solved by future experiments.

3. Information-entropy scaling

As an alternative quantity characterizing the final-state multiplicity distribution P_n, a (momentum-integrated) information entropy can be defined [112, 113] as

$$S = -\sum_n P_n \ln P_n \quad . \tag{15}$$

It is a measure of the uncertainty associated with a multiplicity distribution. A wide distribution gives more uncertainty and a larger value of S than a sharply peaked one. Important properties of S are:

(i) This variable describes the general pattern of particle emission. The total entropy produced from ν statistically independent sources (*e.g.* clans or superclusters) is just the sum of entropies of the individual sources:

$$S = \sum_{i=1}^{\nu} S_i \,. \tag{16}$$

(ii) Distortion of the multiplicity scale leaves S invariant, so does insertion of zeros or mutual permutation. In particular, in full phase space, the entropy is the same when calculated from all charged particles or negatives (*i.e.* charged pairs) only.

(iii) From the identity

$$S - \ln\langle n\rangle = -\frac{1}{\langle n\rangle} \sum \langle n\rangle P_n \ln(\langle n\rangle P_n) \tag{17}$$

follows for large $\langle n\rangle$

$$S - \ln\langle n\rangle = \frac{1}{c} \int_0^{\infty} \psi(z) \ln \psi(z) dz \tag{18}$$

with $\psi(z)$ normalized as

$$\int \psi(z)dz = \int z\psi(z)dz = c \,, \tag{19}$$

where $c = 2$ for all charged particles and $c = 1$ for negatives (or pairs).

(iv) For the geometric distribution $\psi(z) = \exp(-z)$, an upper bound is

$$S - \ln\left(\frac{\langle n\rangle}{c}\right) \leq 1 \,, \tag{20}$$

so that at high enough $\sqrt{s}$

$$\langle n\rangle \simeq (\sqrt{s})^{\kappa} \,.$$

As is shown in Fig. 3.1(a), at high energies ($\sqrt{s} \gtrsim 20$ GeV), the value of S increases linearly with $\ln\sqrt{s}$ [113]. Extrapolating back, the intercept is near $\ln m_\pi$. Since the maximum rapidity is $y_{\max} = \ln(\sqrt{s}/m_\pi)$, it follows that the entropy per rapidity unit $\kappa \equiv S/y_{\max}$ is constant. This constancy is indeed observed up to Tevatron energies [78, 81, 114] with $\kappa = 0.437 \pm 0.004$.

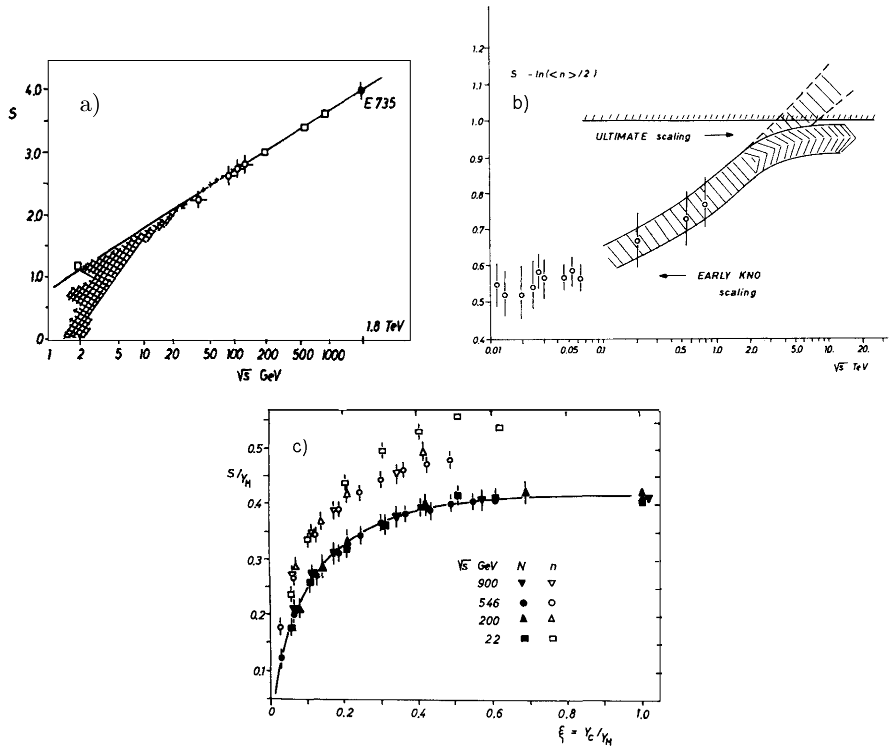

Fig. 3.1. (a) Entropy of the charged-particle multiplicity distribution as a function of $\sqrt{s}$, (b) entropy of $\psi(z)$ from (20) as a function of $\sqrt{s}$, (c) entropy per unit rapidity for rapidity windows $\xi_{\rm cut}$ [113].

From Fig. 3.1(b) it is clear that the limit (20) is not reached at present collider energies. However, at LHC the multiplicity distribution must be governed by (20): either the entropy increase of Fig. 3.1(a) must slow down, or $\langle n \rangle$ must grow faster than presently indicated.

Furthermore, approximate scaling is observed for the function $\kappa(\xi)$ between NA22 at $\sqrt{s} = 22$ GeV and CDF at 1800 GeV [81, 113], when n is restricted to negatives (or the number of oppositely charged pairs), with $\xi = y_{\rm c}/y_{\rm max}$ and $y_{\rm c}$ being half the size of a central rapidity window (Fig. 3.1(c)).

From the constancy of κ for full phase space, one can conclude that the entropy per rapidity unit does not depend on energy. From the shape of the scaling function $\kappa(\xi)$ follows that the entropy reaches its full-phase-space value κ at ξ=0.5, where $\bar{n}$ and k of the negative binomial are still changing. So, the fragmentation region does not contribute to entropy production.

It is interesting to note that the increase in multiplicity is the main source of entropy of high-energy hadronic matter. The entropy of transverse momentum and rapidity increases much slower than $\ln\langle n\rangle$:

$$\begin{aligned} S_{p_{\mathrm{T}}} &\approx \ln\langle p_{\mathrm{T}}\rangle\,, \\ S_y &\approx \ln y_{\max} \approx \ln\ln\sqrt{s}\,. \end{aligned}$$

In hadron–nucleus collisions, an extra contribution ΔS_A to the entropy of negative particles comes from a fluctuating number of nucleons participating [113]. Indeed $\Delta S_{\mathrm{Ne}} = 0.3 \pm 0.05$ is observed for hNe collisions, independent of energy. Also heavy-ion collisions show a similar S-behavior [115,116] with a fast increase of S in the central rapidity region and a rapid saturation of $S/y_{\max}$ above $\xi = 0.4$. The results suggest that, with increasing energy, the entropy per pion saturates.

There are hints that this behavior can be understood from cascading processes [117]. The question remains, how heavy-ion collisions behave w.r.t. the additivity of entropy as observed in hA collisions, and whether entropy differences can be used as a signature for a quark-gluon plasma.

Entropy scaling is an interesting concept, but, contrary to KNO or log-KNO scaling where a whole function is considered, it only concerns the energy independence of one single number.

The information entropy S can be generalized [113] to the Rényi order-q information entropy

$$H_q = \frac{1}{1-q}\ln\sum_n (P_n)^q\,, \quad \text{with } H_1 = S\,, \tag{21}$$

and κ to $D_q = H_q/y_{\max}$. Also the D_q turn out to be approximately energy independent. Comparing hadron–hadron to e^+e^- data, one observes a small but significant difference ($D_q(\mathrm{hh}) > D_q(e^+e^-)$), increasing with increasing order q.

In order to measure higher-order (Rényi) entropies, an originally chosen phase-space region is divided into M equal-size bins [118]. An event is then characterized by the number of particles m_i in each bin i, *i.e.*, by a set of integer numbers $s \equiv m_i$, $i = 1, \ldots M$. These sets represent different states of the multiparticle system realized in a given experiment.

The basis of the method is the measurement of coincidence probabilities, *i.e.*, in simply counting the number n_s of times any given set s appears in the given event sample. The total number of observed coincidences of k configurations is the q^{th} factorial moment of the n_s distribution,

$$N_k = \sum_s n_s(n_s-1)\ldots(n_s-q+1)\,, \quad k = 1,2,3\ldots \tag{22}$$

with only states with $n_s \geq k$ contributing. The coincidence probability of q configurations is

$$C_k = \frac{N_q}{N(N-1)\dots(N-q+1)}\,, \tag{23}$$

where $N = \sum_s n_s$ is the number of events in the sample, so that $C_1 = 1$.

Rényi entropies [119], defined as

$$H_q \equiv -\frac{\ln C_q}{q-1}\,, \quad q > 1 \tag{24}$$

can then be used to extrapolate to $H_1 \equiv S$, the standard statistical (or Shannon) entropy, Eq. (15). With the proper extrapolation formula, an effective reproduction of S could be achieved for a number of typical multiplicity distributions [118].

The advantage over the standard direct calculation of S is minimization of the statistical error and increase of the stability of the result [144].

However, also the Rényi entropies themselves contain valuable information about the multiparticle system. In principle, the entropies H_k (and from their extrapolation also S) obtained depend on the method of discretization of the momentum spectrum, in particular the binning. If the bins are small enough and if the fluctuations are small (*e.g.* if the system is close to thermal equilibrium), one expects [118] scaling of the form

$$H_q(\ell M) = H_q(M) + \ln \ell\,, \tag{25}$$

with ℓ being the change in bin size. Strong fluctuations, as in cascading, on the other hand, are expected to violate this scaling property.

Furthermore, if performed independently (and simultaneously) in different phase space regions Ω_i, the entropy density distribution over phase space can be determined and the additivity property

$$H_q(\Omega) = H_q(\Omega_1) + H_q(\Omega - \Omega_1) \tag{26}$$

can be verified. Deviations from this property give information about correlations between the different regions. An NA22 analysis is under way, but it would be important to be able to compare to heavy-ion results.

4. Rapidity gap probability

Interesting information on higher-order correlations is contained already in the $n = 0$ bin of the multiplicity distribution in a given phase space (*e.g.* rapidity) bin. With $\langle n \rangle$ as the average number of particles in bin Δy, the probability of detecting no particles in Δy is related to the generating function through

$$P_0(\Delta y) = G(z=-1) \tag{27}$$

and can be used as a generating function for $P_n(\Delta y)$:

$$P_n(\Delta y) = \frac{(-\langle n\rangle)^n}{n!}\left(\frac{\partial}{\partial\langle n\rangle}\right)^n P_0(\Delta y)\,, \tag{28}$$

where the differentiation is carried out with the correlation functions fixed. Its dependence on the (higher-order) cumulants is

$$\ln P_0(\Delta y) = \sum_{q=1}^{\infty}\frac{(-1)^q}{q!}f_q = \sum_{q=1}^{\infty}\frac{(-\langle n\rangle)^q}{q!}K_q\,, \tag{29}$$

thus involving cumulants of all orders. Applying the so-called linked-pair ansatz to the normalized cumulant moments K_q [120] gives

$$K_q = A_q K_2^{q-1}\,. \tag{30}$$

If the linking coefficients A_q are independent of $\sqrt{s}$ and Δy, as confirmed by the analysis of UA1 and UA5 data up to $q=5$ [120], then the quantity

$$\chi \;=\; -\ln P_0(\Delta y)/\langle n\rangle \tag{31}$$

$$\;=\; \sum_{q=1}^{\infty}\frac{A_q}{q!}(-\langle n\rangle K_2)^{q-1} = \chi(\langle n\rangle K_2) \tag{32}$$

only depends on the moment product $\langle n\rangle K_2$ [121].

Note that $\langle n\rangle = -\ln P_0(\Delta y)$ for the Poisson distribution, so that χ measures the amount of deviation from independent emission, involving correlations of all orders. The scaling feature was in fact already derived in [122] for the study of void probability in galaxy clustering, where this scaling is found to hold and χ is found to follow $A_q = (q-1)!$, *i.e.* is equal to the linking parameters of the NBD, $\chi = \ln(1+\langle n\rangle K_2)/(\langle n\rangle K_2)$ [123].

In high energy collisions, the scaling was shown to hold [121] in the NA22 hydrogen- and nuclear-target data for $\Delta y < 1$ and χ agrees with the NBD expectation up to $\langle n\rangle K_2 \approx 1$, but falls below for larger values.

A systematic study of P_0 values of UA5 in various central and non-central rapidity bins [78] was done in [124] (Fig. 4.1(a)). Contrary to the galaxy data of [123], most of the points fall somewhat below the NBD expectation (dashed), in agreement with the increase of the linking parameters being somewhat weaker than expected by the NBD [120]. In general, they, however, stay above the full line, representing the simple case of $A_q = 1$

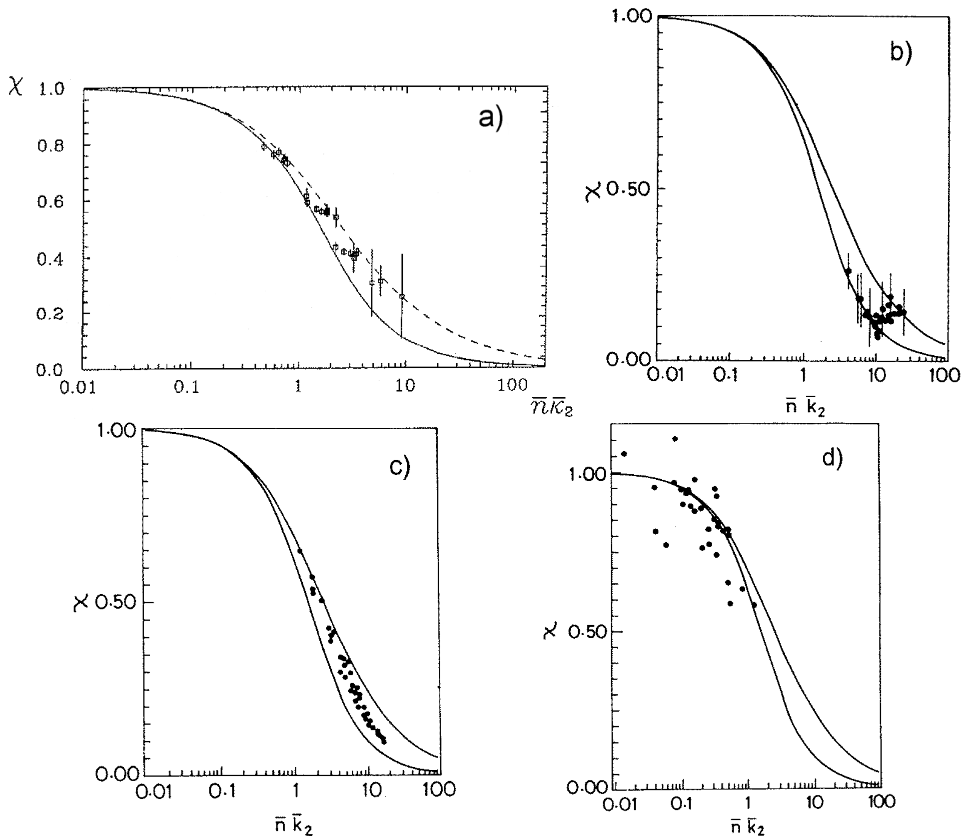

Fig. 4.1. Scaled rapidity gap probability χ as a function of $\langle n\rangle K_2$ for (a) UA5 data [124], (b) ^{16}O-AgBr, (c) FRITIOF and (d) independent emission at 60 A GeV [125]. The upper curve corresponds to the NBD, the lower one to the minimal model.

for all q ("minimal model"). The strongest deviation from the NBD scaling curve appears for the most non-central rapidity bins indicating violation of translation invariance of the correlation.

The UA5 data are scarce and have large errors for $\langle n\rangle K_2 \gtrsim 3$. This region has been extended to 30 in [125] from heavy-ion collisions at 60 AGeV (Fig. 4.1(b))and 200 AGeV. Again, the results lie between the scaling curves expected from NBD and from the minimal model. The authors also compared to the expectations from FRITIOF (Fig. 4.1(c)) and from random production of particles in η-space (Fig. 4.1(d)). While FRITIOF lies within the region bounded by the NBD and the minimal model, be it distributed over a wider $\langle n\rangle K_2$ range than the data, random particle production is limited to $\langle n\rangle K_2 < 1$ and scattered over a wide range in χ, showing no scaling.

5. Forward-backward correlations

The correlation between the charged-particle multiplicity in one hemisphere with that in the other was studied in a wide range of $\sqrt{s}$, from lowest-energy bubble chamber experiments to the Tevatron, and for all types of collisions. Examples are NA22 [126], NA27 [127], the ISR [128], UA5 [129], E735 [130], ν [131,132], EMC [133], TASSO [87,134], HRS [86,135], DELPHI [88], OPAL [136], ZEUS [137].

The average charged-particle multiplicity $\langle n_{\mathrm{F}} \rangle$ in the forward hemisphere is given as a function of the charged-particle multiplicity n_{B} in the backward hemisphere for the NA22 experiment [126] in Fig. 5.1. A comparison to three low p_{T} models shows that the single-chain Lund model, which reproduces the e^+e^- data at comparable energies [134,135] does not reproduce the *hh* data at all. The two-chain FRITIOF and a two-chain version of the Dual Parton Model slightly overestimate the correlation. In all three models oscillations are visible between odd and even n_{B}.

In Fig. 5.1(b), the same distributions are shown, but now for $(--)$, $(+-)$ and $(++)$ charge combinations, separately. The correlation is dominated by unlike-charged particles (note the difference in scale). All three models are able to reproduce the $(+-)$ *hp* data, while FRITIOF I does quite well also for $(--)$ and $(++)$. For the latter, an anti-correlation is expected from Lund. The e^+e^- results can be reproduced by the JETSET PS model. From Fig. 5.1(c), one can see that the correlation is not completely gone when the influence from short-range order is suppressed by eliminating the central region.

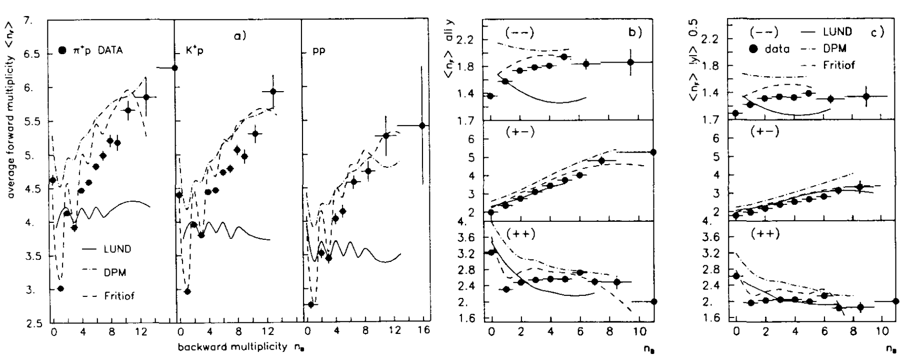

Fig. 5.1. (a) The average number of charged forward particles *versus* the number of charged backward particles for π^+p, K^+p and *pp* collisions at $\sqrt{s}$=22 GeV, with MC predictions as indicated. (b) The same for different charge combinations in the combined data sample. (c) Same for particles with $|y| > 0.5$ [126].

The actual range of the correlation in hh collisions is investigated by the UA5 collaboration [129], who give the slope b defined from

$$\langle n_{\mathrm{B}} \rangle = a + b n_{\mathrm{F}} \tag{33}$$

for two windows of one unit in pseudo-rapidity as a function of the size of the gap separating them. From Fig. 5.2(a) it is clear that a correlation persists up to a gap size of $\Delta\eta = 6$. This (long-range) correlation effect can be well reproduced by the UA5 Cluster Monte Carlo [129] of Poisson-like clusters and a negative binomial total charged-particle multiplicity. It can also be reproduced by the upgraded version of FRITIOF and reasonably well by DPM, but is overestimated in PYTHIA. The energy dependence of this effect between 22 and 900 GeV is given in Fig. 5.2(b) [126].

Forward–backward correlations, and in particular differences found for hh and e^+e^- collisions, are expected and discussed in the geometrical models [138–140].

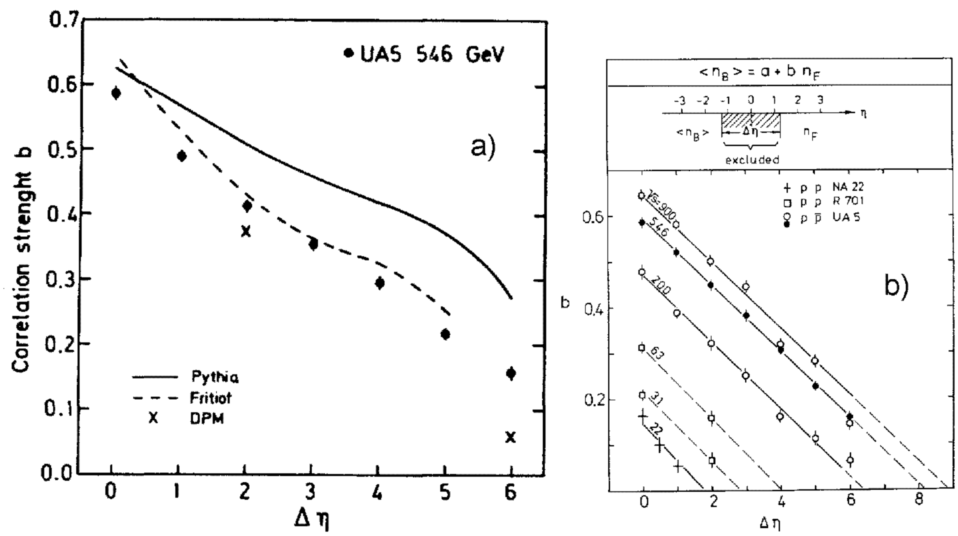

Fig. 5.2. The forward–backward correlation strength b as a function of an excluded central gap $\Delta\eta$ (a) for UA5 [129] (b) for the energies indicated [126].

In Fig. 5.3, a compilation is given for the correlation strength b in hh, lh and e^+e^- collisions, when no central region is excluded. For hh collisions (Fig. 2.5(a)) an approximately linear rise of b is found with increasing $\ln s$ with no saturation, so far. As for $1/k$ in Fig. 2.5, the slope b is lower for lh collisions in Fig. 2.5(b) than for hh collisions, but the energy dependence is the same, at least up to the highest values of W available. Furthermore, b is lower for e^+e^- than for hh and lh collisions and the energy dependence is flatter.

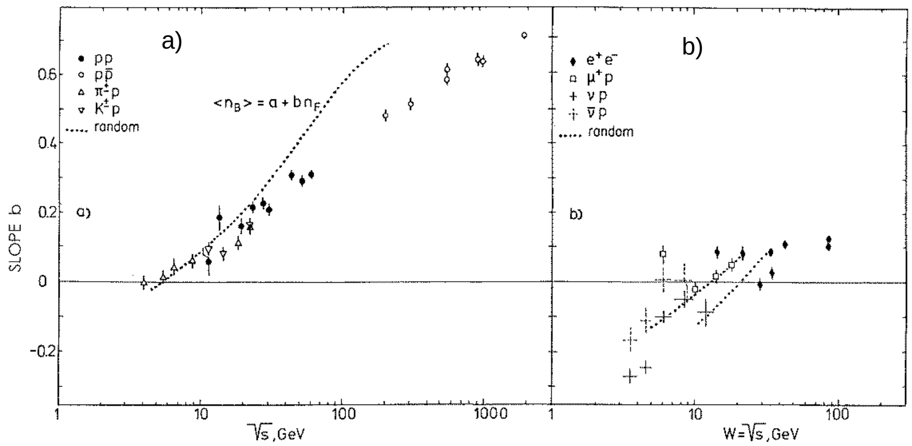

Fig. 5.3. Compilation of the values of the correlation strength b for (a) hh, (b) lh and e^+e^- collisions, as a function of $\sqrt{s}$ and W, respectively [126]. The lines are obtained from those in Fig. 2.5 via Eq. (34).

This is not completely unexpected. If particle production follows a negative binomial with no further correlations from conservation laws or dynamics, $1/k$ and b are related [103, 141] by

$$b = \frac{\frac{\langle n_{\rm B} \rangle}{k}}{1 + \frac{\langle n_{\rm F} \rangle}{k}} \,. \tag{34}$$

The curves derived from the fits in Fig. 2.5 are drawn in Fig. 2.11. Relative to the overall negative binomial, there is an *anti-correlation* building up at high energy in hh collisions. This deviation can be expected if particles are produced in clusters [103, 141] or pairs [142, 143]

From the increase of $1/k$ in Fig. 2.5, a positive slope b is also expected for higher energy lh and e^+e^- collisions. This is shown by the dashed lines in Fig. 5.3(b). Indeed, the TASSO [87], DELPHI [88] and OPAL [136] points are well above $b = 0$, thus establishing positive forward–backward correlations in e^+e^- collisions, as well.

We conclude

1. The energy evolution of the average multiplicity is similar for all types of collisions.

2. For all types of collisions, the multiplicity distribution gets wider than Poisson (*i.e.* correlations exist) above a certain transition energy depending on type of collision and rapidity interval. At given energy, multiplicity distributions are wider for hh than for lh collisions and wider for lh than for e^+e^- collisions.

3. For all types of collisions, in full phase space as well as in limited regions of it, the negative binomial is a surprisingly successful parametrization of the multiplicity distribution, but important deviations exist. The latter have stimulated work on a large variety of extensions and alternatives.

4. Up to the highest energy reached so far, KNO scaling neither holds for full-phase-space multiplicity distributions, nor for multiplicity distributions in limited intervals. For all types of collisions, a log-scaling law may be an interesting candidate for a replacement. Also entropy scaling should be further investigated.

5. Positive forward-backward correlations exist for all types of collisions at energies above the Poissonian transition point. At given energy, they are stronger in *hh* than in *lh* collisions and stronger in *lh* than in e^+e^- collisions. They grow with increasing energy, but less fast than would be expected from the widening of the negative binomial. For *hh* collisions at Collider energies, they are positive over a gap of at least 6 units in rapidity.

6. The momentum correlations and density fluctuations

6.1. The formalism

We start by defining symmetrized inclusive q-particle distributions

$$\rho_q(p_1, \ldots, p_q) = \frac{1}{\sigma_{\mathrm{tot}}} \frac{d\sigma_q(p_1, \ldots, p_q)}{\prod\limits_1^q dp_q}, \tag{35}$$

where $\sigma_q(p_1, \ldots, p_q)$ is the inclusive cross section for q particles to be at $p_1, \ldots, p_q$, irrespective of the presence and location of any further particles, p_i is the (four-) momentum of particle i and σ_{tot} is the total hadronic cross section of the collision under study. For the case of identical particles, integration over an interval Ω in p-space yields

$$\begin{aligned} &\int\limits_\Omega \rho_1(p)dp = \langle n \rangle\,, \quad \int\limits_\Omega \int\limits_\Omega \rho_2(p_1, p_2)dp_1 dp_2 = \langle n(n-1) \rangle\,, \\ &\int\limits_\Omega dp_1 \ldots \int\limits_\Omega dp_q \rho_q(p_1, \ldots, p_q) = \langle n(n-1)\ldots(n-q+1) \rangle\,, \end{aligned} \tag{36}$$

where n is the multiplicity of identical particles within Ω in a given event and the angular brackets imply the average over the event ensemble.

Besides the interparticle *correlations* we are looking for, the inclusive q-particle number densities $\rho_q(p_1, \ldots, p_q)$ in general contain "trivial" contributions from lower-order densities. It is, therefore, advantageous to consider a new sequence of functions $C_q(p_1, \ldots, p_q)$ as those statistical quantities which vanish whenever one of their arguments becomes statistically independent of the others [145–147]:

$$C_2(1,2) = \rho_2(1,2) - \rho_1(1)\rho_1(2)\,, \tag{37}$$

$$C_3(1,2,3) = \rho_3(1,2,3) - \sum_{(3)} \rho_1(1)\rho_2(2,3) + 2\rho_1(1)\rho_1(2)\rho_1(3)\,, \tag{38}$$

etc. In the above relations, we have abbreviated $C_q(p_1, \ldots, p_q)$ to $C_q(1, 2, \ldots, q)$; the summations indicate that all possible permutations must be taken. Expressions for higher orders can be derived from the related formulae given in [148]. Deviations of these functions from zero shall be addressed as *genuine* correlations.

It is often convenient to divide the functions ρ_q and C_q by the product of q one-particle densities, which leads to the definition of the normalized inclusive densities and correlations:

$$R_q(p_1, \ldots, p_q) = \rho_q(p_q, \ldots, p_q)/\rho_1(p_1)\ldots\rho_1(p_q)\,, \tag{39}$$

$$K_q(p_1, \ldots, p_q) = C_q(p_1, \ldots, p_q)/\rho_1(p_1)\ldots\rho_1(p_q)\,. \tag{40}$$

In terms of these functions, correlations have been studied extensively for $q = 2$. Results also exist for $q = 3$, but usually the statistics (*i.e.* number of events available for analysis) are too small to isolate genuine correlations. To be able to do that for $q \geq 3$, one must apply factorial moments F_q defined via the integrals in Eq. (37), but in limited phase-space cells [149, 150].

6.2. Density spikes

To see whether it is worth the effort, we first look for density fluctuations in single events, signalling high-order correlations. A notorious JACEE event [151] at a pseudo-rapidity resolution (binning) of $\delta\eta = 0.1$ has local fluctuations up to $dn/d\eta \approx 300$ with a signal-to-background ratio of about 1:1. An NA22 event [152] contains a "spike" at a rapidity resolution $\delta y = 0.1$ of $dn/dy = 100$, as much as 60 times the average density in this experiment.

Bialas and Peschanski [149] suggested that this type of spikes could be a manifestation of "intermittency", a phenomenon well known in fluid dynamics [153]. The authors argued that if intermittency indeed occurs in particle production, large density fluctuations are not only expected, but should also exhibit self-similarity with respect to the size of the phase-space volume.

Ideas on self-similarity and fractals in jet physics had already been formulated in [154, 155]. For soft hadronic processes, fractals and self-similarity were first considered in [156] and their quantitative measures in [157].

In multiparticle experiments, the number of hadrons produced in a single collision is small and subject to considerable noise. To exploit the techniques employed in complex-system theory, a method had to be devised to separate fluctuations of purely statistical (Poisson) origin, due to finite particle numbers, from the possibly self-similar dynamical fluctuations of the underlying particle densities. A solution, already used in quantum optics [158] and suggested for multiparticle production in [149], consists in measuring $F_q(\delta y)$ in given phase-space volumes (resolution) δy of ever decreasing size.

Note, however, that this approach of explicitely eliminating "trivial" effects is recently being complemented by a more "holistic" approach [159].

6.3. Power-law scaling

Besides the property of noise-suppression, high-order factorial moments act as a filter and resolve the large-multiplicity tail of the multiplicity distribution. They are thus particularly sensitive to large density fluctuations at the various scales δy used in the analysis. As shown in [149], a smooth density distribution, which does not show any fluctuations except for the statistical ones, has the property of normalized factorial moments $F_q(\delta y)$ being independent of the resolution δy in the limit $\delta y \to 0$. On the other hand, if self-similar dynamical fluctuations exist, the F_q obey the power law

$$F_q(\delta y) \propto (\delta y)^{-\phi_q}\,, \quad (\delta y \to 0)\,. \tag{41}$$

The powers ϕ_q (slopes in a double-log plot) are related [160] to the anomalous (or co-) dimensions $d_q = \phi_q/(q-1)$, a measure for the deviation from an integer dimension. Equation (41) is a scaling law since the ratio of the factorial moments at resolutions L and ℓ

$$R = \frac{F_q(\ell)}{F_q(L)} = \left(\frac{L}{\ell}\right)^{\phi_q} \tag{42}$$

only depends on the ratio L/ℓ, but not on L and ℓ, themselves.

One further has to stress the advantages of normalized factorial cumulants K_q compared to factorial moments, since the former measure *genuine* correlation patterns.

As an example, high statistics data of the OPAL experiment [161] are given in Fig. 6.1 in terms of K_q, as a function of the number $M \propto 1/\delta y$ of phase space partitions for $q = 3$ to 5. In the leftmost column, the one-dimensional rapidity variable y is used for the analysis. The data (black dots) show an increase of K_q with increasing M for small M, but a saturation at larger M. Even though weaker, some saturation still persists when the analysis is done in the two-dimensional plane of rapidity y and azimuthal angle φ (middle column), but approximate power-law scaling is indeed observed for the analysis in three-dimensional momentum space (right column). Thus, in high-energy collisions, fractal behavior is fully developed in three dimensions, while projection effects lead to saturation in lower dimension.

In Fig. 1, the data are also compared to a number of parametrizations of the multiplicity distributions, as well as to the Monte Carlo models JETSET and HERWIG. One can see that the fluctuations given by the negative binomial (NB) (dashed line) are weaker than observed in the data. Contrary to the NB, the log-normal (LN) distribution (dotted line) overestimates the cumulants, while these expected for a pure birth (PB) process (dash-dotted) underestimate the data even more significantly than the NB. Among the distributions shown, a modified NB (MNB) gives the best results, even though significant underestimation is observed also there. The Monte Carlo models do surprisingly well.

6.4. Density and correlation integrals

A fruitful development in the study of density fluctuations is the density and correlation strip-integral method. [162] By means of integrals of the inclusive density over a strip domain in y_1, y_2 space, rather than a sum of box domains, one not only avoids unwanted side-effects such as splitting of density spikes, but also drastically increases the integration volume (and therefore the statistical significance) at given resolution. In terms of the strips (or hyper-tubes for $q > 2$), the density integrals can be evaluated directly from the data after selection of a proper distance measure, as *e.g.* the four-momentum difference $Q^2_{ij} = -(p_i - p_j)^2$, and after definition of a proper multiparticle topology (GHP integral, [162] snake integral, [163] star integral [164]). Similarly, *correlation* integrals can be defined by replacing the density ρ_q in the integral by the correlation function C_q.

Of particular interest is a comparison of hadron–hadron to e^+e^- results in terms of same and opposite charges of the particles involved. Such a comparison is shown in Fig. 6.2 for $q = 2$. An important difference between UA1 and DELPHI can be observed in a comparison of the two sub-figures: For relatively large $Q^2 (> 0.03\ \mathrm{GeV}^2)$, where Bose-Einstein effects do not play a major role, the e^+e^- data increase much faster with increasing $-_2 \log Q^2$ than the hadron–hadron results. For e^+e^-, the increase in this Q^2 region is very similar for same and for opposite-sign charges. At small Q^2, however, the e^+e^- results approach the hh results. For e^+e^- annihilation at LEP at least two processes are responsible for the power-law behavior: Bose–Einstein correlation at small Q^2 following the evolution of jets at larger Q^2.

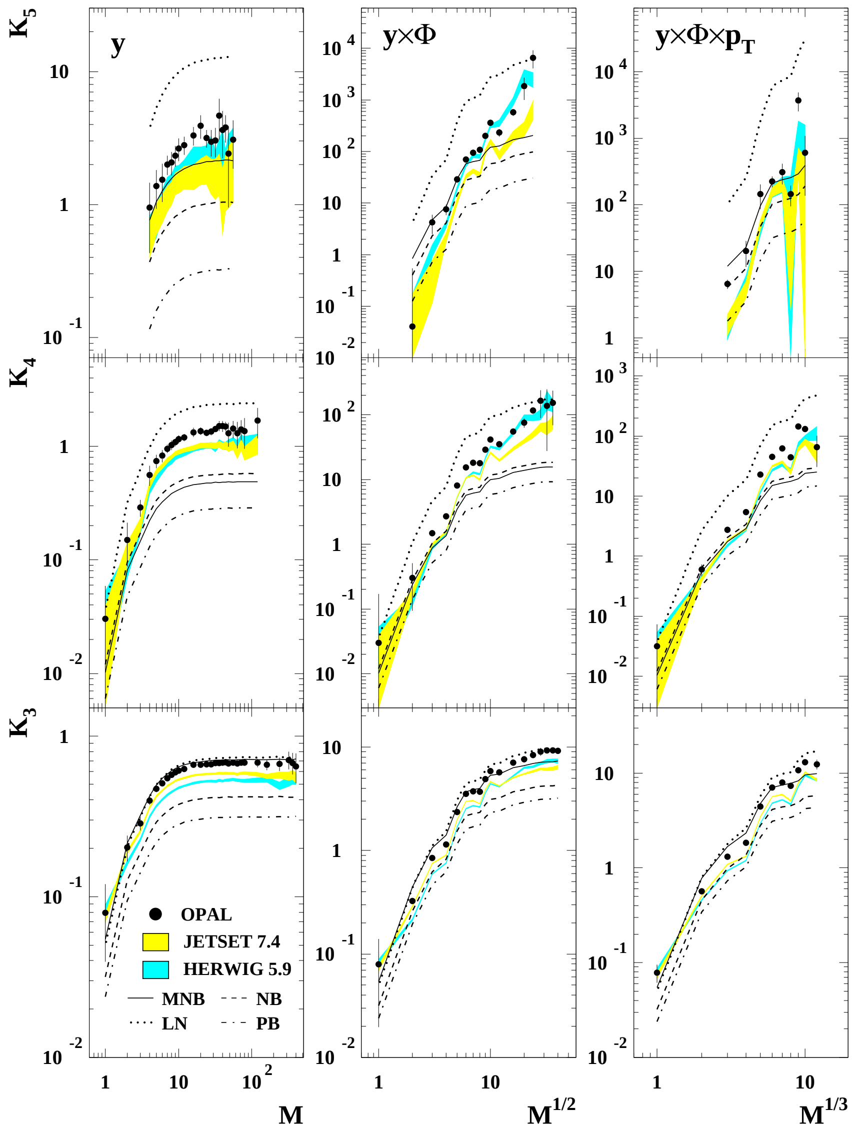

Fig. 6.1. Cumulants of order $q = 3$ to 5 as a function of $M^{1/D}$ in comparison with the predictions of various multiplicity parametrizations and two Monte Carlo models [161].

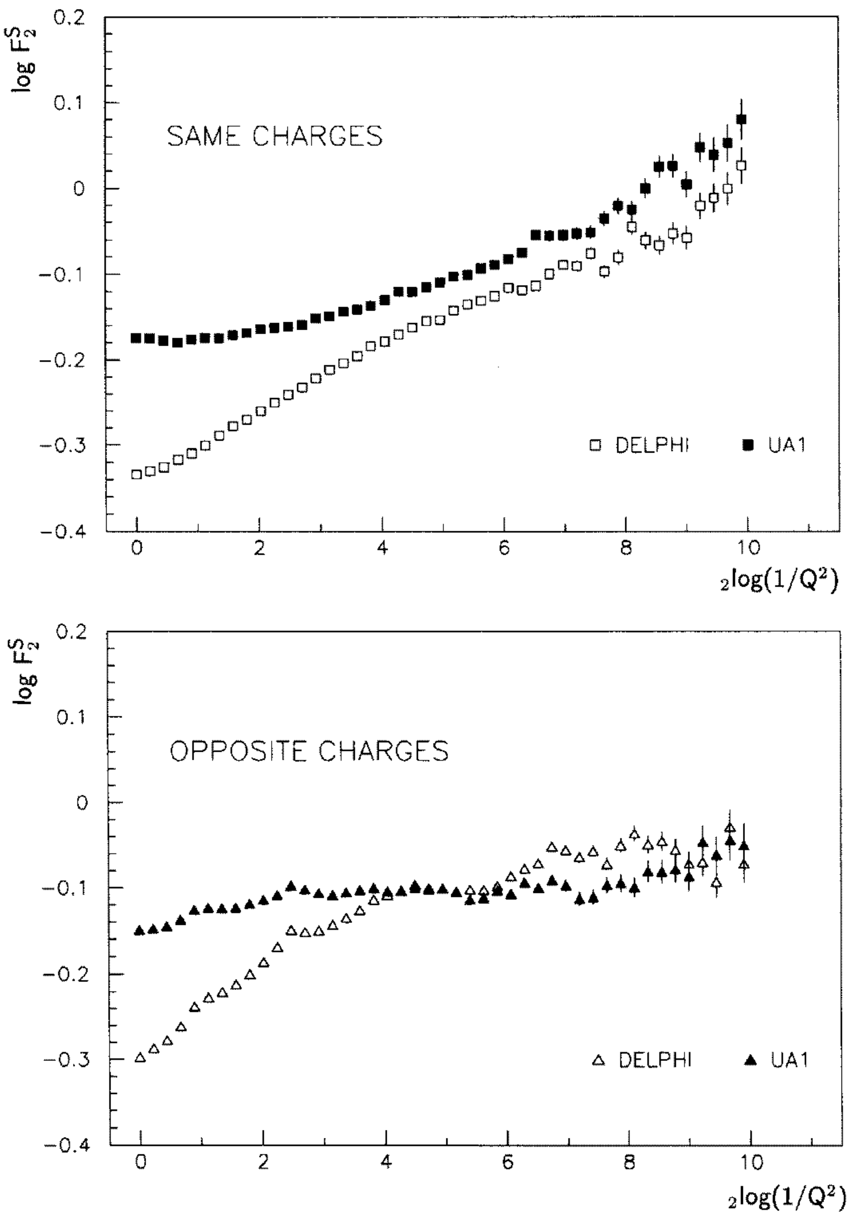

Fig. 6.2. Comparison of density integrals for $q = 2$ in their differential form ΔF_2 (in intervals $Q^2, Q^2 + dQ^2$) as a function of $_2\log(1/Q^2)$ for e^+e^- (DELPHI) and hadron–hadron collisions (UA1). [166]

6.5. Multifractal versus monofractal behavior

Anomalous dimensions d_q fitted over the (one-dimensional) range $0.1 < \delta y < 1.0$ are compiled in Fig. 6.3 [170]. They typically range from $d_q = 0.01$ to 0.1, which means that the fractal (Rényi) dimensions $D_q = 1 - d_q$ are close to one. The d_q are larger and grow faster with increasing order q in μp and e^+e^- (Fig. 6.3(a)) than in hh collisions (Fig. 6.3(b)) and are small and almost independent of q in heavy-ion collisions (Fig. 6.3(c)). For hh collisions, the q-dependence is considerably stronger for NA22 ($\sqrt{s} = 22$ GeV, all p_{T}) than for UA1 ($\sqrt{s} = 630$ GeV, $p_{\mathrm{T}} > 0.15$ GeV/c).

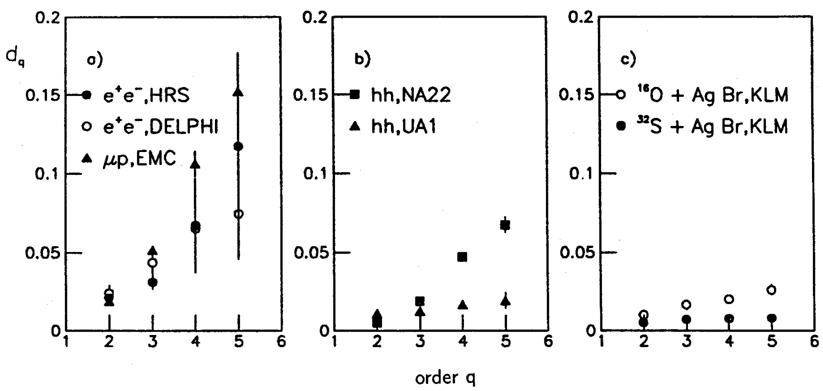

Fig. 6.3. Anomalous dimension d_q as a function of the order q, for (a) μp and e^+e^- collisions, (b) NA22 and UA1, (c) KLM [170].

In multiplicative cascade models, the one-dimensional moments follow the generalized power law [171]

$$F_q \propto (g(\delta y))^{\phi_q} \,, \tag{43}$$

where $g(\delta y)$ is a general function of δy. Expressing g in terms of F_2, one finds the linear relation

$$\ln F_q = c_q + \left(\frac{\phi_q}{\phi_2}\right) \ln F_2 \,, \tag{44}$$

from which the ratio of anomalous dimensions is directly obtained. This has been confirmed by experiment, not only in one dimension, but up to 3D [172]. Moreover, the ratios ϕ_q/ϕ_2 are found to be largely independent of the dimension of phase space and of the type of collision. The q dependence is indicative of the mechanism causing intermittent behavior. For a (multiplicative) cascade mechanism, in the log-normal approximation (long cascades), the moments satisfy the relation

$$\frac{d_q}{d_2} = \frac{\phi_q}{\phi_2}\frac{1}{q-1} = \frac{q}{2}\,. \tag{45}$$

However, the use of the Central Limit Theorem for a multiplicative process, such as in the α-model, is a very crude approximation [173] particularly in the tails. As argued in [174], a better description is obtained if the density probability distribution is assumed to be a log-Lévy-stable distribution, characterized by a Lévy index μ. In that case (45) generalizes to

$$\frac{d_q}{d_2} = \frac{1}{2^\mu - 2}\frac{q^\mu - q}{q-1}\,. \tag{46}$$

For $\mu = 0$, implying an order-independent anomalous dimension, the multifractal behavior characterized by (45)–(46) reduces to a monofractal behavior [175, 176] with $d_q/d_2 = 1$. This would happen if intermittency were due to a second-order phase transition.

The data are best fitted with a Lévy index of $\mu = 1.6$, but important exceptions exist: While a fit to the combined NA22 data [177] on all variables and dimensions, as well as a weighted average over all individual fits give μ values in rough agreement with those of [172], the 3D-data have $\mu > 2$, not allowed in the sense of Lévy laws. Even larger values of μ, ranging from 3.2 to 3.5, have been found for μp deep-inelastic scattering in [174].

6.6. Self-affinity versus self-similarity

Comparing log-log plots for one phase-space dimension, one notices that the $\ln F_q$ saturate, but at different F_q values for different variables y, φ or $\ln p_{\mathrm{T}}$. However, also in three-dimensional analysis the power law is not exact. The 3D hh data even bend upward. It has been shown in [181] that this can be understood by taking the anisotropy of occupied phase space into account. In view of this phase-space anisotropy, also its partition should be anisotropic. If the power law holds when space is partitioned by the same factor in different directions, the fractal is called *self-similar*. If, on the other hand, it holds and only holds when space is partitioned by different factors in different directions, the corresponding fractal is called *self-affine* [182].

If the phase-space structure is indeed self-affine, it can be characterized by a parameter called roughness or Hurst exponent [182], defined as

$$H_{ij} = \frac{\ln M_i}{\ln M_j} \quad (0 \le H_{ij} \le 1) \tag{47}$$

with M_i ($i = 1,2,3;\quad M_1 \le M_2 \le M_3$) being the partition numbers in the self-affine transformations $\delta y_i \to \delta y_i/M_i$, of the phase-space variables y_i.

The Hurst exponents can be obtained [181] from the experimentally observed saturation curves of the one-dimensional $F_2(\delta y_i)$ distributions,

$$F_2^i(M_i) = A_i - B_i M_i^{-\gamma_i} \tag{48}$$

as $H_{ij} = (1+\gamma_j)/(1+\gamma_i)$. For hh collisions, H_{ij} was indeed determined to be of order 0.5 [183] for the longitudinal-transverse combinations, while it was found consistent with unity within the transverse plane $(\varphi, p_{\mathrm{T}})$.

The anisotropy is consistent with the fact that the longitudinal direction is privileged over the transverse directions in hadron–hadron collisions. On the contrary, no upward bending is observed in the three-dimensional self-similar analysis of e^+e^- data [184], so the H_{ij} are expected to be compatible with unity. This observation is confirmed with the help of a full self-affine analysis performed with a JETSET 7.4 Monte-Carlo sample at 91.2 GeV [185] and a full analysis of L3 data is underway [186] indicating an approximately self-similar behavior for full e^+e^- events, but a self-affine one for single jets.

7. Local fluctuations and QCD

Substantial progress has been made to derive analytical QCD predictions for fluctuations [167–169] in small angular phase-space intervals. Assuming LPHD [187], these predictions for the parton level can be compared to experimental data [188–190]. QCD is inherently intermittent and QCD predictions [167–169] grant the scaling behavior

$$F_q(\Theta) \propto \left(\frac{\Theta_0}{\Theta}\right)^{(D-D_q)(q-1)}, \tag{49}$$

where Θ_0 is the half opening angle of a cone around the jet-axis, Θ is the angular half-width of a ring around the jet-axis centered at Θ_0, D is the underlying topological dimension ($D = 1$ for single angle Θ), and D_q are the Rényi dimensions.

A new scaling variable [169], $z = \ln(\Theta_0/\Theta)/\ln(E\Theta_0/\Lambda)$, where the maximum possible region ($\Theta = \Theta_0$) corresponds to $z = 0$, is used in Fig. 6.1(a). In a fixed coupling regime, for moderately small angular bins,

$$D_q = \gamma_0(Q)\frac{q+1}{q}, \tag{50}$$

where $\gamma_0(Q) = \sqrt{2\,C_{\mathrm{A}}\alpha_{\mathrm{s}}(Q)/\pi}$ is the anomalous QCD dimension calculated at $Q \simeq E\Theta_0$, $E = \sqrt{s}/2$, and gluon color factor $C_{\mathrm{A}} = N_{\mathrm{c}} = 3$. This corresponds to the thin solid lines in Fig. 7.1(a). In the running-coupling regime, for small bins, the Rényi dimensions become a function of the size of the angular ring ($\alpha_s(Q)$ increases with decreasing Θ). Three approximations derived in DLLA are compared in Fig. 7.1(a), according to (a) [168], (b) [169], (c) [167]. In [168], an estimate for D_q has, furthermore, been obtained in MLLA.

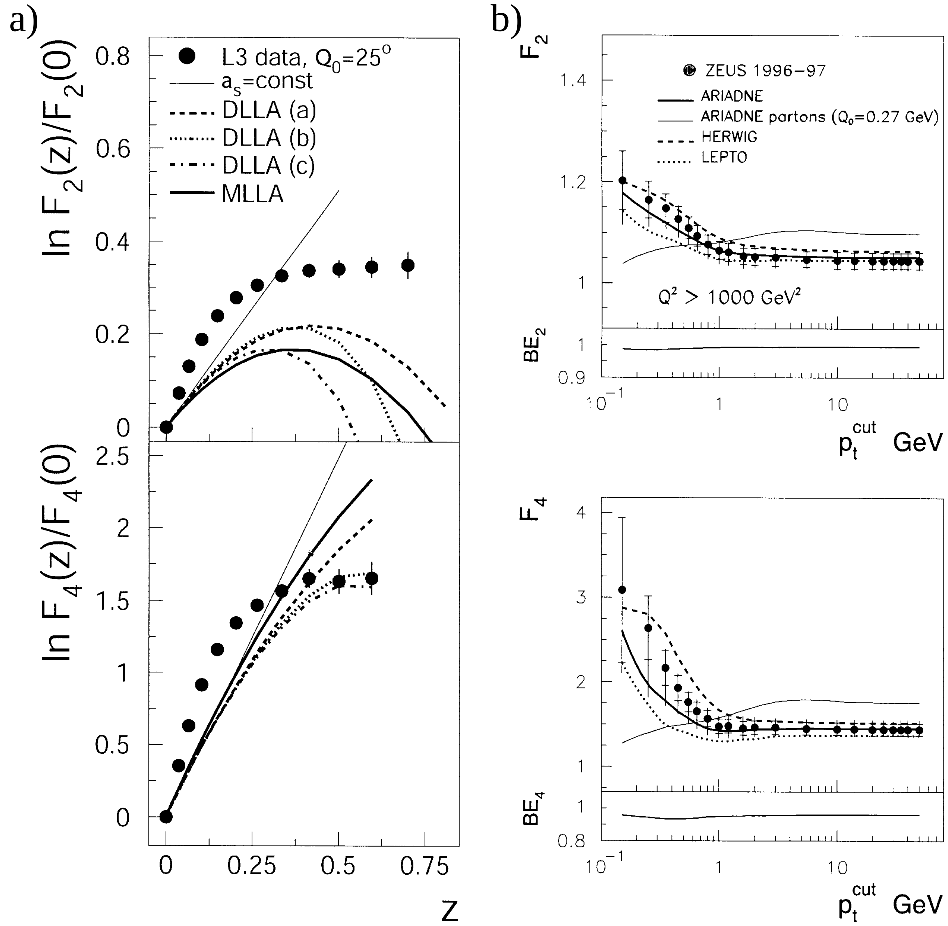

Fig. 7.1. (a) The L3 data [189] compared to the analytical QCD predictions for $\Lambda = 0.16$ GeV and $\Theta_0 = 25^0$: $\alpha_s = \text{const}$ (thin solid line); DLLA (a) [168]; DLLA (b) [169]; DLLA (c) [167]; MLLA [168]. b) Factorial moments for charged particles in the current region of the Breit frame of e^+p collisions at HERA, as a function of p_t^{cut}, compared to Monte-Carlo models at the hadron level (thick lines) and ARIADNE with $Q_0 = 0.27$ GeV at the parton level (thin solid line). The data are corrected for Bose-Einstein correlations by the BE factor indicated [192].

The fixed coupling approximates the running coupling for small z, but does not exhibit the saturation effect seen in the data. For second order, the running-α_s predictions lead to the saturation effects observed in the data, but significantly underestimate the observed signal. Predictions for the higher moments are too low for low values of z, but tend to overestimate the data at larger z. The DLLA approximation differs significantly at large z. The MLLA predictions do not differ significantly from the DLLA result.

Using transverse momentum p_t rather than Θ, within DLLA, the normalized factorial moments of gluons which are restricted as $p_T < p_T^{cut}$ are expected [191] to follow,

$$F_q(p_T^{cut}) \simeq 1 + \frac{q(q-1)}{6} \frac{\ln(p_T^{cut}/Q_0)}{\ln(P/Q_0)}\,, \tag{51}$$

where P is again the initial energy of the outgoing quark and p_T is defined relative to the direction of this quark.

Again, the DLLA predictions are on the parton level and should be regarded asymptotic, *i.e.* valid at small p_T^{cut}. Therefore, they should be considered only as qualitative predictions when compared to the data in conjungation with the LPHD hypothesis. Such a comparison has been made by ZEUS [192] (see Fig. 7.1(b)). While DLLA (Eq. (51)) predicts the moments to approach unity from above as p_T^{cut} decreases, the data show the opposite. The Monte-Carlo models follow the trend of the data, with ARIADNE giving the best overall description.

To check the effect of energy-momentum conservation, the moments were also determined at the parton level of ARIADNE, the physics implementation of which strongly resembles the analytic calculations [191]. To satisfy LPHD, the cut-off parameter Q_0 was reduced to 0.27 GeV, also ensuring the parton multiplicity to equal that of the hadrons. The results are given as the thin solid line in Fig. 7.1(b). They indeed show the behavior expected from Eq. (51), *i.e.*, they disagree with the hadronic data. Analogous differences between the hadron and parton levels of ARIADNE have been observed in e^+e^- annihilation [191]. So, one has to conclude with the authors that here the limits of LPHD are crossed, *i.e.* the F_q are particularly sensitive to dynamical details of non-perturbative QCD.

8. Bose–Einstein Correlations

Whether derived as Fourier transform of a (static and chaotic) pion source distribution, a covariant Wigner-transform of the (momentum dependent) source density matrix, or from the string model, identical-pion correlation leads to a positive, non-zero two-particle correlator $K_2(Q)$ (see

Eqs. (40) and (41)), *i.e.* to

$$R_2(Q) = 1 + K_2(Q) > 1 \tag{52}$$

at small four-momentum difference Q. These Bose–Einstein Correlations, by now, are a well-established effect in all types of collisions, even in hadronic Z^0 decay (for recent reviews see [193, 194]) originally expected to be too coherent to show an effect. If existent also as inter-W BEC in fully hadronic WW decay at LEP2, this could serve as an important laboratory for research on the behavior of two (partially) overlapping strings.

Other important recent observations are given in abstract from below.

1. When evaluated in two (or better three) dimensions in the Bertsch–Pratt system, an *elongation* of the emission region (better region of homogeneity [195] is observed along the event axis in all types of collisions (hadron–hadron [196], all four LEP experiments [197], ZEUS [198], RHIC [199]). However, it is important to note that the longitudinal radius of homogeneity is much shorter than the length of the sting (of order 1%).

The recent observation that the out-radius does not grow beyond the side-radius at RHIC [199] points to a short duration of emission and causes a problem for some hydrodynamical models, but not for *e.g.* the Buda–Lund hydro model. The latter, in fact gives a beautifully consistent description of single-particle spectra and BEC in hadron–hadron and heavy-ion collisions at SPS and RHIC [200]. The emission function resembles a Gaussian shaped fire-ball for AA collisions, but a fire-tube for hh collisions.

2. The form of the correlator at small Q is steeper than Gaussian, in fact consistent with a power law as would be expected from the intermittency phenomenon described above. Recent unifying progress is reported in [201].

3. The approximate $m_{\mathrm{T}}^{-1/2}$ scaling first observed in heavy-ion collisions at the SPS [202] and usually blamed on collective flow, is now observed at RHIC [203], but also in e^+e^- collisions [204]. Quite generally, it follows from a strong position momentum correlation [205], be it due to collective flow or to string fragmentation.

4. *Genuine three-pion correlations* exist in all types of collisions and, in principle, allow a phase to be extracted from

$$\cos\phi \equiv \omega(Q_3) = K_3(Q_3)/2\sqrt{K_2(Q_3)}\,. \tag{53}$$

At small Q, this ω is near unity (as expected from incoherence) for hh [206] and e^+e^- [207] collisions, as well as for PbPb [208, 209] and AuAu [210] collisions at SPS and RHIC, while it is near zero (compatible with full coherence) in collisions of light nuclei [208]. This contradiction can be solved [193, 211] if ω is interpreted as a ratio of normalized cumulants (Eq. (41)). Since $K_q^{(N)}$ of N independent overlapping sources gets diluted like $1/N^{q-1}$, ω would be reduced if strings produced by light ions (or in WW decay!) do not interact. If, in *heavy* ion collisions, the string density gets high enough for them to coalesce, some kind of percolation sets in and full inter-string BEC gets restored.

5. Azimuthal anisotropy is now also observed in configuration space of non-central heavy-ion collisions at AGS energies [212], but also at RHIC [213]. Contrary to elliptic flow, it is directed out of the event plane, but consistent with the elliptic nuclear overlap in a non-central collision. Due to larger pressure in the event plane, the anisotropy gets reduced but not destroyed at RHIC. Also this is evidence for a short duration of pion emission.

Since a reaction plane also exists in hA, hh, and three-jet e^+e^- collisions, application to those would be interesting. Of course, a three-dimensional analysis in Φ bins requires a very high statistics.

9. Summary

Since conclusions were already given at the end of the individual sections, we will not repeat them here, but limit ourselves to a comment. Multiparticle production in high-energy collisions is an ideal field to study genuine higher-order correlations. They are directly accessible in their full multidimensional characteristics, under well controlled experimental conditions. Methods also used in other fields are being tested and extended here for general application. Indications for genuine, approximately self-similar higher-order correlations are indeed found in high-energy particle collisions. At large four-momentum distance Q^2, they are not only expected to be an inherent property of perturbative QCD, but are directly related to the anomalous multiplicity dimension and, therefore, to the running coupling constant α_s. At small Q^2, the QCD effects are complemented by Bose–Einstein interference of identical mesons carrying information on the unknown space-time development of particle production during the collision. The interplay between these two mechanisms, important for an understanding of the process of hadronization, is a particular challenge at the moment.

REFERENCES

[1] M. Adamus *et al.* [NA22 Coll.], *Z. Phys.* **C39**, 311 (1988).

[2] J. Benecke, T.T. Chou, C.N. Yang, F. Yen, *Phys. Rev.* **188**, 2159 (1969); T.T. Chou, C.N. Yang, *Phys. Rev. Lett.* **25**, 1072 (1970); *Phys. Rev.* **D50**, 590 (1994).

[3] G. Bellettini *et al.*, *Phys. Lett.* **45B**, 69 (1973).

[4] R.P. Feynman, *Phys. Rev. Lett.* **23**, 1415 (1969).

[5] G. Alner *et al.* [UA5 Coll.], *Z. Phys.* **C33**, 1 (1986).

[6] F. Abe *et al.* [CDF Coll.], *Phys. Rev.* **D41**, 2330 (1990).

[7] B. Andersson, G. Gustafson, C. Peterson, *Phys. Lett.* **69B**, 221(1977); *Phys. Lett.* **71B**, 337 (1977); B. Andersson, G. Gustafson, I. Holgersson, O. Mansson, *Nucl. Phys.* **B178**, 242 (1981); B. Andersson, G. Gustafson, G. Ingelman, T. Sjöstrand, *Phys. Rep.* **97**, 31 (1983).

[8] G. Gustafson, *Phys. Lett.* **B175**, 453 (1986); G. Gustafson, U. Pettersson, *Nucl. Phys.* **B306**, 746 (1988).

[9] A. Capella, U. Sukhatme, C.I. Tan, J. Tran Thanh Van, *Phys. Lett.* **81B**, 68 (1979); *Z. Phys.* **C3**, 329 (1980); *Phys. Rep.* **236**, 225 (1994); G. Cohen-Tannoudji, F. Hayot, R. Peschanski, *Phys. Rev.* **D17**, 2930 (1978); G. Cohen-Tannoudji *et al.*, *Phys. Rev.* **D21**, 2699 (1980); H. Minakata, *Phys. Rev.* **D20**, 1656 (1979); M. Bishari, G. Cohen-Tannoudji, H. Navelet, R. Peschanski, *Z. Phys.* **C14**, 7 (1982); G. Cohen-Tannoudji *et al.*, *Z. Phys.* **C13**, 219 (1982).

[10] R. Holynski, Cracow report INP 1303/PH (1986).

[11] B.B. Back *et al.* [PHOBOS Coll.], *Phys. Rev. Lett.* **91**, 052303 (2003).

[12] A. Bialas, M. Jezabek, *Phys. Lett.* **B590**, 233 (2004).

[13] M.C. Abreu *et al.* [NA50 Coll.], *Phys. Lett.* **B530**, 43 (2002); B.B. Bark *et al.* [PHOBOS Coll.], *Phys. Rev. Lett.* **85**, 3100 (2000); K. Adcox *et al.* [PHENIX Coll.], *Phys. Rev. Lett.* **86**, 3500 (2001); I.G. Bearden *et al.* [BRAHMS Coll.], *Phys. Lett.* **B523**, 227 (2001); *Phys. Rev. Lett.* **88**, 202301 (2002).

[14] C. Albajar *et al.* [UA1 Coll.], *Nucl. Phys.* **B335**, 261 (1990).

[15] T. Alexopoulos *et al.* [E735 Coll.], *Phys. Rev. Lett.* **60** 1622 (1988), *Phys. Rev.* **D48**, 984 (1993); *Phys. Lett.* **B336**, 599 (1994).

[16] F. Abe *et al.* [CDF Coll.], *Phys. Rev. Lett.* **61**, 1819 (1989).

[17] E.A. De Wolf,*Proc. XV-th Int. Symp. on Multiparticle Dynamics, Lund*, ed. G. Gustafson, World Scientific, Singapore 1984, p. 2.

[18] W. Bell *et al.*, *Z. Phys.* **C27**, 191 (1985).

[19] H. Ströbele *et al.* [NA35 Coll.], *Z. Phys.* **C38**, 89 (1988).

[20] C.M.G. Lattes, Y. Fujimoto, S. Hasegawa, *Phys. Rep.* **65**, 151 (1980).

[21] G. Arnison *et al.* [UA1 Coll.], *Phys. Lett.* **B118**, 167 (1982).

[22] T.H. Burnett *et al.* [JACEE Coll.], *Phys. Rev. Lett.* **57**, 3249 (1986).

[23] R.E. Ansorge *et al.* [UA5 Coll.], *Z. Phys.* **C41**, 179 (1988).

[24] T. Åkesson *et al.*, *Phys. Lett.* **B119**, 464 (1982).

[25] A. Breakstone *et al.* [SFM Coll.], *Phys. Lett.* **B132**, 463 (1983); *Z. Phys.* **C33**, 333 (1987); *Phys. Lett.* **B183**, 227 (1987); *Europhys. Lett.* **7**, 131 (1988).

[26] L. Van Hove, *Phys. Lett.* **B118**, 138 (1982); R. Hagedorn, *Rivista Nuovo Cimento* **6-10**, (1983) 1; R. Campanini, *Nuovo Cimento Lett.* **44**, 343 (1985).

[27] P. Levai, B. Müller, *Phys. Rev. Lett.* **67**, 1519 (1991).

[28] S. Barshay, *Phys. Lett.* **B127**, 129 (1983); *Phys. Rev.* **D29**, 1010 (1984).

[29] M. Jacob, CERN preprint TH-3515 (1983).

[30] G. Pancheri, C. Rubbia, *Nucl. Phys.* **A418**, 117C (1984); G. Pancheri, Y. Srivastava, M. Pallotta, *Phys. Lett.* **151B**, 453 (1985); G. Pancheri, Y. Srivastava, *Phys. Lett.* **B159**, 69 (1985).

[31] F.W. Bopp, P. Aurenche, J. Ranft, *Phys. Rev.* **D33**, 1867 (1986).

[32] X.N. Wang, R.C. Hwa, *Phys. Rev.* **D39**, 187 (1989); X.N. Wang, M. Gyulassy, *Phys. Rev.* **D45**, 844 (1992), *Phys. Lett.* **B282**, 466 (1992).

[33] V.V. Aivazyan *et al.* [NA22 Coll.], *Phys. Lett.* **B209**, 103 (1988).

[34] R. Akers *et al.* [OPAL Coll.], *Phys. Lett.* **B320**, 417 (1994).

[35] P. Abreu *et al.* [DELPHI Coll.], *Phys. Lett.* **B276**, 254 (1992).

[36] M. Szczekowski, G. Wilk, *Phys. Rev.* **D44**, R577 (1991).

[37] G. Arnison *et al.* [UA1 Coll.], *Nucl. Phys.* **B276**, 253 (1986).

[38] K. Althoff *et al.* [TASSO Coll.], *Z. Phys.* **C22**, 307 (1984).

[39] J. Breitweg *et al.* [ZEUS Coll.], *Eur. Phys. J.* **C8**, 367 (1999).

[40] J. Pernegr, V. Šimák, M. Votruba, *Nuovo Cim.* **17**, 129 (1960); M. Bardadin *et al.*, *Proc. Sienna Conf. on Elem. Part.* (1963), p. 628.

[41] M. Althoff *et al.*, *Z. Phys.* **C22**, 307 (1984).

[42] M. Derrick *et al.*, *Phys. Rev.* **D17**, 1 (1978); P. Allen *et al.*, *Nucl. Phys.* **B188**, 1 (1981); D. Allasia *et al.*, *Z. Phys.* **C27**, 239 (1985).

[43] M. Arneodo *et al.* [EMC Coll.], *Phys. Lett.* **B149**, 415 (1984); *Z. Phys.* **C35**, 417 (1987); *Z. Phys.* **C36**, 527 (1987).

[44] Ph. Herquet *et al.*, *Properties of Jet-Like Systems Observed in π^+p, K^+p and pp Interactions*, Proc. XVth Renc. de Moriond 1980, Vol. I, ed. J. Tran Than Van, Editions Frontières, 1980, p. 215.

[45] P. Hoyer *et al.*, *Nucl. Phys.* **B161**, 34 (1979); A. Ali *et al.*, *Z. Phys.* **C2**, 33 (1979).

[46] B. Andersson, G. Gustafson, T. Sjöstrand, *Phys. Lett.* **B94**, 211 (1980).

[47] E. Stone *et al.*, *Phys. Rev.* **D5**, 1621 (1972); I.V. Ajinenko *et al.*, *Z. Phys.* **C4**, 181 (1980); M. Barth *et al.*, *Z. Phys.* **C7**, 187 (1981).

[48] A. Borg *et al.*, *Nucl. Phys.* **B106**, 430 (1976); J.M. Laffaille *et al.*, *Nucl. Phys.* **B192**, 18 (1981).

[49] I.V. Ajinenko *et al.* [NA22 Coll.], *Phys. Lett.* **B197**, 457 (1987).

[50] D. Drijard *et al.*, *Z. Phys.* **C9**, 293 (1981).

[51] P.V. Chliapnikov, V.A. Uvarov, *Phys. Lett.* **B345**, 313 (1995); **B381**, 483 (1996); **B423**, 401 (1998); P.V. Chlipanikov, *Phys. Lett.* **B462**, 341 (1999); **B470**, 263 (1999); **B525**, 1 (2002); V. Uvarov, *Phys. Lett.* **B482**, 10 (2000), **B511**, 136 (2001).

[52] N.M. Agababyan *et al.* [NA22 Coll.], *Z. Phys.* **C41**, 539 (1989).

[53] M. Adamus *et al.* [NA22 Coll.], *Phys. Lett.* **B198**, 427 (1987); I.V. Ajinenko *et al.*, *Z. Phys.* **C44**, 573 (1989); N.M. Agababyan *et al.*, *Z. Phys.* **C46**, 525 (1990).

[54] M. Bardadin-Otwinowska *et al.*, *Nucl. Phys.* **B98**, 418 (1975).

[55] F. Barreiro *et al.*, *Nucl. Phys.* **B126**, 319 (1977).

[56] H. Grässler *et al.*, *Nucl. Phys.* **B118**, 189 (1977).

[57] K. Böckmann *et al.*, *Nucl. Phys.* **B140**, 235 (1978).

[58] W. Ochs, *Nucl. Phys.* **B118**, 397 (1977).

[59] J. Singh *et al.*, *Nucl. Phys.* **B140**, 189 (1978).

[60] A. Wróblewski, *Proc. XIV Int. Symp. on Multiparticle Dynamics, Lake Tahoe*, ed. P. Yager, J.F. Gunion, World Scientific, Singapore 1984, p. 573.

[61] S. Barlag *et al.*, *Z. Phys.* **C11**, 283 (1982); M. Derrick *et al.*, *Phys. Rev.* **D25**, 624 (1982); H. Grässler *et al.*, *Nucl. Phys.* **B223**, 269 (1983).

[62] C. Bacci *et al.*, *Phys. Lett.* **B86**, 234 (1979); J.L. Siegrist *et al.*, *Phys. Rev.* **D26**, 969 (1982); B. Niczyporuk *et al.*, *Z. Phys.* **C9**, 1 (1981); M.S. Alam *et al.*, *Phys. Rev. Lett.* **49**, 357 (1982); Ch. Berger *et al.*, *Phys. Lett.* **B95**, 313 (1980); W. Bartel *et al.*, *Z. Phys.* **C20**, 187 (1983).

[63] P.V. Chliapnikov, V.A. Uvarov, *Phys. Lett.* **B251**, 192 (1990).

[64] A. Bassetto, M. Ciafaloni, G. Marchesini, *Phys. Lett.* **B83**, 207 (1979); *Nucl. Phys.* **B163**, 477 (1980); W. Furmanski, R. Petronzio, S. Pokorski, *Nucl. Phys.* **B155**, 253 (1979).

[65] M. Bardadin-Otwinowska, M. Szczekowski, A.K. Wróblewski, *Z. Phys.* **C13**, 83 (1982).

[66] Z. Koba, H.B. Nielsen, P. Olesen, *Nucl. Phys.* **B40**, 317 (1972).

[67] G.J. Alner *et al.* [UA5 Coll.], *Phys. Lett.* **B138**, 304 (1984).

[68] H. Müller, *Proc. 25th Int. Conf. on High Energy Physics*, eds. K.K. Phua, Y. Yamaguchi, South East Asia Theor. Phys. Assoc., Singapore 1991, p. 872.

[69] M. Garetto, A. Giovannini, *Lett. Nuovo Cim.* **7**, 35 (1973); A. Giovannini *et al.*, *Nuovo Cim.* **24A**, 421 (1974); N. Suzuki, *Prog. Theor. Phys.* **51**, 1629 (1974); W.J. Knox, *Phys. Rev.* **D10**, 65 (1974).

[70] G.J. Alner *et al.* [UA5 Coll.], *Phys. Lett.* **B160**, 199 (1985).

[71] G.J. Alner *et al.* [UA5 Coll.], *Phys. Lett.* **B160**, 193 (1985).

[72] G.J. Alner *et al.* [UA5 Coll.], *Phys. Lett.* **B167**, 476 (1986).

[73] M. Adamus *et al.* [NA22 Coll.], *Phys. Lett.* **B177**, 239 (1986); *Z. Phys.* **C32**, 475 (1986); *Z. Phys.* **C37**, 215 (1988).

[74] R. Ammar *et al.* [LEBC-MPS Coll.], *Phys. Lett.* **B178**, 124 (1986).

[75] C. De Marzo *et al.* [NA5 Coll.], *Phys. Rev.* **D26**, 1019 (1982); F. Dengler *et al.*, *Z. Phys.* **C33**, 187 (1986).

[76] J.L. Bailly *et al.* [NA23 Coll.], *Z. Phys.* **C40**, 215 (1988).

[77] A. Breakstone *et al.* [SFM Coll.], *Nuovo Cim.* **102A**, 1199 (1989).

[78] R.E. Ansorge *et al.* [UA5 Coll.], *Z. Phys.* **C43**, 357 (1989).

[79] A.O. Bouzas *et al.* [E735 Coll.], *Z. Phys.* **C56**, 107 (1992); T. Alexopoulos *et al.*, *Phys. Lett.* **B435**, 453 (1998).

[80] J. Bächler *et al.* [NA35 Coll.], *Z. Phys.* **C57**, 541 (1993).

[81] F. Rimondi [CDF Coll.], *Proc. XXIII Int. Symp. on Multiparticle Dynamics, Aspen 1993*, eds. M. Block, A. White, World Scientific, Singapore 1994, p. 400; F. Abe *et al.*, *Phys. Rev.* **D50**, 5550 (1994).

[82] H.J. Tannenbaum [E802 Coll.], *Mod. Phys. Lett.* **A9**, 89 (1994); T. Abbott *et al.*, *Phys. Rev.* **C52**, 2663 (1995).

[83] M. Arneodo *et al.* [EMC Coll.], *Z. Phys.* **C35**, 335 (1987).

[84] D. Allasia *et al.* [WA29 Coll.], DFUB 88/9 (1988).

[85] S. Aid *et al.* [H1 Coll.], *Z. Phys.* **C72**, 573 (1996).

[86] M. Derrick *et al.* [HRS Coll.], *Phys. Lett.* **B168**, 299 (1986); *Phys. Rev.* **D34**, 3304 (1986).

[87] W. Braunschweig *et al.* [TASSO Coll.], *Z. Phys.* **C45**, 193 (1989).

[88] P. Abreu *et al.* [DELPHI Coll.], *Z. Phys.* **C50**, 185 (1991); *Z. Phys.* **C52**, 271 (1991); *Z. Phys.* **C56**, 63 (1992).

[89] P.D. Acton *et al.* [OPAL Coll.], *Z. Phys.* **C53**, 539 (1992).

[90] D. Decamp *et al.* [ALEPH Coll.], *Phys. Lett.* **B273**, 181 (1991); D. Buskulic *et al.*, *Z. Phys.* **C69**, 15 (1995).

[91] P. Carruthers, C.C. Shih, *Int. J. Mod. Phys.* **A2**, 1447 (1987); A. Giovannini, *Proc. XXVI Int. Symp. on Multiparticle Dynamics, Faro 1996*, eds. J. Dias de Deus *et al.*, World Scientific, Singapore 1997, p. 232.

[92] A. Giovannini, L. Van Hove, *Z. Phys.* **C30**, 391 (1986); L. Van Hove, A. Giovannini, *Proc. of XVII Int. Symp. on Multiparticle Dynamics, Seewinkel (1986)*, eds. M. Markytan *et al.*, World Scientific, Singapore 1987, p. 561.

[93] R. Szwed, G. Wrochna, *Z. Phys.* **C29**, 255 (1985); R. Szwed, G. Wrochna, A.K. Wróblewski, *Acta Phys. Pol. B* **19**, 763 (1988); *Mod. Phys. Lett.* **A5**, 1851 (1990); **A6**, 245 (1991); S. Carius, G. Ingelman, *Phys. Lett.* **B252**, 647 (1990).

[94] A. Giovannini, R. Ugoccioni, *Phys. Rev.* **D59**, 094020 (1999); J. Dias de Deus, R. Ugoccioni, *Phys. Lett.* **B469**, 243 (1999).

[95] T. Mizoguchi, M. Biyajima, G. Wilk, *Phys. Lett.* **B301**, 131 (1993); M. Biyajima *et al.*, *Phys. Lett.* **B515**, 470 (2001).

[96] S.G. Matinyan, W.D. Walker, *Phys. Rev.* **D59**, 034022 (1999).

[97] V.D. Rusov *et al.*, *Phys. Lett.* **B504**, 213 (2001).

[98] J. Huskins, *Nucl. Phys.* **B46**, 547 (1972); P. Olesen, *Nucl. Phys.* **B47**, 157 (1972).

[99] W. Ochs, *Proc. XX Int. Symp. On Multiparticle Dynamics, Gut Holmecke 1990*, eds. R. Baier, D. Wegener, World Scientific, Singapore 1991, p. 434.

[100] A.M. Polyakov, *Sov. Phys. JETP* **32**, 296 (1971); **33**, 850 (1971); S.J. Orfanidis, V. Rittenberg, *Phys. Rev.* **D10**, 2892 (1974); W. Ochs, *Z. Phys.* **C23**, 131 (1984); G. Cohen-Tannoudji, W. Ochs, *Z. Phys.* **C39**, 513 (1988).

[101] K. Alpgård *et al.* [UA5 Coll.], *Phys. Lett.* **B121**, 209 (1983).

[102] C. Albajar *et al.* [UA1 Coll.], *Nucl. Phys.* **B335**, 261 (1990).

[103] W.A. Zajc, *Phys. Lett.* **B175**, 219 (1986).

[104] W. Kittel, *Proc. Workshop on Physics with Future Accelerators, La Thuile 1987*, ed. J. Mulvey, CERN 87-7, Vol. II., p. 424.

[105] H.-U. Bengtsson, *Comput. Phys. Commun.* **31**, 323 (1984); H.-U. Bengtsson, G. Ingelman, *Comput. Phys. Commun.* **34**, 251 (1985); H.-U. Bengtsson, T. Sjöstrand, *Comput. Phys. Commun.* **46**, 43 (1987); T. Sjöstrand, *Comput. Phys. Commun.* **27**, 243 (1982); **28**, 227 (1983); **39**, 347 (1986); **82**, 74 (1994); T. Sjöstrand, M. Bengtsson, *Comput. Phys. Commun.* **43**, 367 (1987); T. Sjöstrand *et al.*, *Comput. Phys. Commun.* **135**, 238 (2001).

[106] G. Marchesini, B.R. Webber, *Nucl. Phys.* **B310**, 461 (1988); I.G. Knowles, *Nucl. Phys.* **B310**, 571 (1988); *Comput. Phys. Commun.* **58**, 271 (1990); G. Marchesini *et al.*, *Comput. Phys. Commun.* **67**, 465 (1992).

[107] A. Giovannini, L. Van Hove, *Acta Phys. Pol. B* **19**, 495 (1988); L. Van Hove, A. Giovannini, *Acta Phys. Pol. B* **19**, 917, 931 (1988).

[108] O. Czyżewski, K. Rybicki, *Nucl. Phys.* **B47**, 633 (1972); M. Blažek, *Z. Phys.* **C32**, 309 (1986).

[109] S. Hegyi, *Phys. Lett.* **B466**, 380 (1999); **B467**, 126 (1999); *Nucl. Phys., (Proc. Supp.)* **B92**, 122 (2001); *Proc. XXXth Symp. on Multiparticle Dynamics, Tihany*, eds. T. Csörgő *et al.*, World Scientific, Singapore 2001, p. 423.

[110] Yu.L. Dokshitzer, *Phys. Lett.* **B305**, 295 (1993); LU-TP/93-3 (1993).

[111] B. Adeva *et al.* [L3 Coll.], *Z. Phys.* **C55**, 39 (1992).

[112] A. Wehrl, *Rev. Mod. Phys.* **50**, 221 (1978).

[113] V. Šimák, M. Šumbera, I. Zborovský, *Phys. Lett.* **B206**, 159 (1988); M. Pachr, V. Šimák, M. Šumbera, I. Zborovský, *Mod. Phys. Lett.* **A7**, 2333 (1992); *Proc. XIXth Int. Symp. on Multiparticle Dynamics 1988*, eds. D. Schiff, J. Tran Than Van, Editions Frontières, Gif-sur-Yvette 1988, p. 399; *Proc. XXVth Int. Symp. on Multiparticle Dynamics 1995*, eds. D. Bruncko *et al.*, World Scientific, Singapore 1996, p. 617.

[114] T. Alexopoulos *et al.* [E735 Coll.], Multiplicity Distributions of Charged Particles from Proton–Antiproton Collisions at the Tevatron Collider at $\sqrt{s} = 1.8$ TeV, *The Vancouver Meeting, Particles and Fields 1991*, eds. D. Axen, D. Bryman, World Scientific, Singapore p. 748.

[115] D. Ghosh *et al.*, *Canad. J. Phys.* **70**, 667 (1992).

[116] A. Mukhopadhyay *et al.*, *Phys. Rev.* **C47**, 410 (1993).

[117] P. Brogueira, J. Dias de Deus, I.P. da Silva, *Phys. Rev.* **D53**, 5283 (1996).

[118] A. Bialas, W. Czyż, J. Wosiek, *Acta Phys. Pol. B* **30**, 107 (1999); A. Bialas, W. Czyż, *Phys. Rev.* **D61**, 074021 (2000); *Acta Phys. Pol. B* **31**, 687 (2000).

[119] A. Rényi, *Acta Math. Sci. Hung.* **10**, 193 (1959).

[120] P. Carruthers, H.C. Eggers, Q. Gao, I. Sarcevic, *Int. J. Mod. Phys.* **A6**, 3031 (1991); P. Carruthers, H.C. Eggers and I. Sarcevic, *Phys. Lett.* **B254**, 258 (1991).

[121] E.A. De Wolf, *Proc. Ringberg Workshop on Multiparticle Production*, eds. R.C. Hwa *et al.*, World Scientific, Singapore 1992, p. 222.

[122] S.D.M. White, *Mon. Not. R. Astron. Soc.* **186**, 145 (1979).

[123] J. Fry, R. Giovanelli, M.P. Haynes, A. Molott, R.J. Scherrer, *Astrophys. J.* **340**, 11 (1989).

[124] S. Hegyi, *Phys. Lett.* **B274**, 214 (1992).

[125] D. Ghosh *et al.*, *Astroparticle Phys.* **15**, 329 (2001); Multiparticle Production in ^{16}O-AgBr Interaction at 60 A GeV — Evidence of Void Probability Scaling, Jadavpur preprint 2000.

[126] V.V. Aivazyan *et al.* [NA22 Coll.], *Z. Phys.* **C42**, 533 (1989).

[127] Yuanxiu Ye *et al.*, *Phys. Lett.* **B382**, 196 (1996).

[128] S. Uhlig *et al.*, *Nucl. Phys.* **B132**, 15 (1978).

[129] K. Alpgård *et al.* [UA5 Coll.], *Phys. Lett.* **B123**, 361 (1983); G.J. Alner *et al.*, *Nucl. Phys.* **B291**, 445 (1987); R.E. Ansorge *et al.*, *Z. Phys.* **C37**, 191 (1988).

[130] T. Alexopoulos *et al.* [E735 Coll.], *Phys. Lett.* **B353**, 155 (1995).

[131] H. Grässler *et al.* [ABBCLMO Coll.], *Nucl. Phys.* **B223**, 269 (1983).

[132] D. Zieminska, *Phys. Rev.* **D27**, 502 (1983).

[133] M. Arneodo *et al.* [EMC Coll.], *Nucl. Phys.* **B258**, 249 (1985).

[134] M. Althoff *et al.* [TASSO Coll.], *Z. Phys.* **C29**, 347 (1985).

[135] M. Derrick *et al.* [HRS Coll.], *Z. Phys.* **C35**, 323 (1987).

[136] R. Akers *et al.* [OPAL Coll.], *Phys. Lett.* **B320**, 417 (1994).

[137] J. Breitweg *et al.* [ZEUS Coll.], *Euro. Phys. J.* **C12**, 53 (2000).

[138] S. Barshay, *Nucl. Phys.* **238**, 277 (1984); *Z. Phys.* **C32**, 513 (1986); *Mod. Phys. Lett.* **A2**, 693 (1987); **A6**, 55 (1991); S. Barshay, E. Eich, *Phys. Lett.* **B178**, 431 (1986); *Mod. Phys. Lett.* **A1**, 459 (1986).

[139] T.T. Chou, C.N. Yang, E. Yen, *Phys. Rev. Lett.* **54**, 510 (1985); T.T. Chou, C.N. Yang, *Phys. Rev.* **D32**, 1692 (1985).

[140] A. Giovannini, *Nucl. Phys.* **B161**, 429 (1979); C.S. Lam, M.A. Walton, *Phys. Lett.* **B140**, 246 (1984); D.C. Hinz, C.S. Lam, *Phys. Rev.* **D33**, 3256 (1986); R.C. Hwa, C.S. Lam, *Phys. Lett.* **B173**, 346 (1986); C.S. Lam, *Proc. 21st Rencontre de Moriond* (1986), ed. J. Tran Thanh Van, Editions Frontières, Vol.II, p. 241; C.C. Shih, *Phys. Rev.* **D33**, 3391 (1986); **D34**, 2710 (1986); C.K. Chew, D. Kiang, H. Zhou, *Phys. Lett.* **B186**, 411 (1987); R.C. Hwa, *Phys. Rev.* **D37**, 1830 (1988); A.V. Batunin, *Phys. Lett.* **B212**, 495 (1988); A.H. Chan, C.K. Chew, *Nuovo Cim.* **101A**, 409 (1989).

[141] P. Carruthers, C.C. Shih, *Phys. Lett.* **B165**, 209 (1985); M. Braun, C. Pajares, V.V. Vechernin, *Phys. Lett.* **B493**, 54 (2000).

[142] Cai Xu, Liu Lian-Shou, *Nuovo Cim. Lett.* **37**, 495 (1983); X. Cai, W. Chao, T. Meng, C. Huang, *Phys. Rev.* **D33**, 1287 (1986); W. Chao, T. Meng, J. Pan, *Phys. Lett.* **B176**, 211 (1986); *Phys. Rev.* **D35**, 152 (1987); *Phys. Rev. Lett.* **58**, 1399 (1987).

[143] M. Biyajima *et al.*, *Z. Phys.* **C44**, 199 (1989).

[144] K. Fialkowski, R. Wit, *Phys. Rev.* **D62**, 114016 (2000).

[145] B. Kahn, G.E. Uhlenbeck, *Physica* **5**, 399 (1938).

[146] K. Huang, *Statistical Mechanics*, John Wiley and Sons, 1963.

[147] A.H. Mueller, *Phys. Rev.* **D4**, 150 (1971).

[148] M.G. Kendall, A. Stuart, *The Advanced Theory of Statistics*, Vol. 1, C. Griffin, Co., London 1969.

[149] A. Bialas, R. Peschanski, *Nucl. Phys.* **B273**, 703 (1986); *Nucl. Phys.* **B308**, 857 (1988); A. Bialas, *Multiparticle Dynamics*, Festschrift Van Hove, eds. A. Giovannini, W. Kittel, World Scientific, Singapore 1990, p. 75.

[150] E.A. De Wolf, I.M. Dremin, W. Kittel, *Phys. Rep.* **270**, 1 (1996).

[151] T.H. Burnett *et al.* [JACEE Coll.], *Phys. Rev. Lett.* **50**, 2062 (1983).

[152] M. Adamus *et al.* NA22 Coll.], *Phys. Lett.* **B185**, 200 (1987).

[153] Ya.B. Zeldovich, A.A. Ruzmaikin, D.D. Sokoloff in *The Almighty Chance*, World Scientific Lecture Notes in Physics, Vol. 20, World Scientific, Singapore 1990.

[154] K. Konishi, A. Ukawa, G. Veneziano, *Phys. Lett.* **78B**, 243 (1978); *Nucl. Phys.* **B157**, 45 (1979).

[155] A. Giovannini, Proc. Xth Int. Symp. on Multiparticle Dynamics, Goa 1979, eds. S.N. Ganguli, P.K. Malhotra, A. Subramanian (Tata Inst.) p. 364.

[156] P. Carruthers, Minh Duong-Van, Evidence for a Common Fractal Dimensionin Turbulence, Galaxy Distributions and Hadronic Multiparticle Production, Los Alamos preprint LA-UR-83-2419, 1983.

[157] I.M. Dremin, *JETP Lett.* **45**, 643 (1987); I.M. Dremin, *Festschrift L. Van Hove*, eds. A. Giovannini, W. Kittel, World Scientific, Singapore 1990, p. 455.

[158] G. Bédard, *Proc. Phys. Soc.* **90**, 131 (1967); D. Cantrell, *Phys. Rev.* **A1**, 672 (1970).

[159] Liu Qin, Meng Ta-chung, *Phys. Rev.* **D69**, 054026 (2004).

[160] P. Lipa, B. Buschbeck, *Phys. Lett.* **B223**, 465 (1989); R. Hwa, *Phys. Rev.* **D41**, 1456 (1990).

[161] E.K.G. Sarkisyan, *Phys. Lett.* **B477**, 1 (2000); I.G. Abbiendi *et al.* [OPAL Coll.], *Phys. Lett.* **523**, 35 (2001).

[162] H.G.E. Hentschel, I. Procaccia, *Physica* **D8**, 435 (1983); P. Grassberger, *Phys. Lett.* **A97**, 227 (1983); I.M. Dremin, *Mod. Phys. Lett.* **A13**, 1333 (1988); P. Lipa *et al.*, *Phys. Lett.* **B285**, 300 (1992).

[163] P. Carruthers, I. Sarcevic, *Phys. Rev. Lett.* **63**, 1562 (1989).

[164] H.C. Eggers *et al.*, *Phys. Rev.* **D48**, 2040 (1993).

[165] N. Neumeister *et al.* [UA1 Collab.], *Z. Phys.* **C60**, 633 (1993).

[166] F. Mandl, B. Buschbeck in *Proc. Cracow Workshop on Multiparticle Production*, eds. A. Bialas *et al.* , World Scientific, Singapore 1994, p.1.

[167] W. Ochs, J. Wosiek, *Phys. Lett.* **B289**, 159 (1992); *Phys. Lett.* **305**, 144 (1993); *Z. Phys.* **C68**, 269 (1995).

[168] Y.L. Dokshitzer, I.M. Dremin, *Nucl. Phys.* **B402**, 139 (1993).

[169] Ph. Brax, J.-L. Meunier, R. Peschanski, *Z. Phys.* **C62**, 649 (1994).

[170] A. Bialas, K. Zalewski, *Nucl. Phys.* **A545**, 345c (1991).

[171] W. Ochs, J. Wosiek, *Phys. Lett.* **B214**, 617 (1988); **B232**, 271 (1989).

[172] W. Ochs, *Phys. Lett.* **B247**, 101 (1990); *Z. Phys.* **C50**, 339 (1991).

[173] J. Alberty, A. Bialas, *Z. Phys.* **C50**, 315 (1991).

[174] Ph. Brax, R. Peschanski, *Phys. Lett.* **B253**, 225 (1991).

[175] H. Satz, *Nucl. Phys.* **B326**, (1989) 613; B. Bambah, J. Fingberg, H. Satz, *Nucl. Phys.* **B332**, 629 (1990).

[176] A. Bialas, R. Hwa, *Phys. Lett.* **B253**, 436 (1991).

[177] I.V. Ajinenko *et al.* [NA22 Coll.], *Phys. Lett.* **B222**, 306 (1989); **B235**, 373 (1990); N.M. Agababyan *et al.*, *Phys. Lett.* **B261**, 165 (1991).

[178] S.P. Ratti *et al.*, *Z. Phys.* **C61**, 229 (1994); S.P. Ratti *et al.* (IHSC), *Proc. XXI Int. Symp. on Multiparticle Dynamics, Wuhan, China, 1991*, eds.Y.F. Wu, L.S. Liu, World Scientific, Singapore 1992, p. 409; V. Arena *et al.* (IHSC), *Nuovo Cim.* **108A**, 417 (1995).

[179] R.C. Hwa, *Phys. Rev.* **D51**, 3323 (1995); Hu Yuan *et al.*, *Chin. Phys. Lett.* **16**, 553 (1999).

[180] Wang Shaoshun, Wu Chong, *Phys. Lett.* **B473**, 172 (2000); *Chin. Phys. Lett.* **18**, 18 (2001).

[181] Y.F. Wu, L.S. Liu, *Phys. Rev. Lett.* **70**, 3197 (1993); *Science in China* **A38**, 435 (1995); Y.F. Wu, Y. Zhang, L.S. Liu, *Phys. Rev.* **D51**, 6576 (1995); Liu Feng, Liu Fuming, Liu Lianshou, *Phys. Rev.* **D59**, 114020 (1999).

[182] B.B. Mandelbrot, in *Dynamics of Fractal Surfaces*, eds. E. Family, T. Vicsek, World Scientific, Singapore 1991.

[183] N.M. Agababyan *et al.* [NA22 Coll.], *Phys. Lett.* **B382**, 305 (1996); *Phys. Lett.* **B431**, 451 (1998).

[184] Liu Lianshou, Zhang Yang, Deng Yue, *Z. Phys.* **C73**, 535 (1997).

[185] Gang Chen, Lian-shou Liu, Yan-min Gao, *Int. J. Mod. Phys.* **A14**, 3687 (1999).

[186] Gang Chen [L3 Coll.], *Proc. XXXI Int. Symp. on Multiparticle Dynamics*, eds. Bai Yuting *et al.*, World Scientific, Singapore 2002, p. 361.

[187] Ya.I. Azimov *et al.*, *Z. Phys.* **C27**, 65 (1985).

[188] P. Abreu *et al.* [DELPHI Coll.], *Phys. Lett.* **B457**, 368 (1999).

[189] M. Acciari *et al.* [L3 Coll.], *Phys. Lett.* **B428**, 186 (1998).

[190] J. Breitweg *et al.* [ZEUS Coll.], *Eur. Phys. J.* **C12**, 53 (2000); S. Chekanov *et al.*, *Phys. Lett.* **510**, 36 (2001).

[191] S. Lupia, W. Ochs, J. Wosiek, *Nucl. Phys.* **B540**, 405 (1999).

[192] S. Chekanov *et al.* [ZEUS Coll.], *Phys. Lett.* **B510**, 36 (2001).

[193] W. Kittel, *Acta Phys. Pol. B* **32**, 3927 (2001).

[194] G. Alexander, *Rep. Prog. Phys.* **66**, 481 (2003).

[195] S.V. Akkelin, Yu.M. Sinyukov, *Phys. Lett.* **B356**, 521 (1995); *Z. Phys.* **C72**, 501 (1996).

[196] N.M. Agababyan *et al.* [NA22 Coll.], *Z. Phys.* **C71**, 405 (1996).

[197] M. Acciari *et al.* [L3 Coll.], *Phys. Lett.* **B458**, 517 (1999); P. Abreu *et al.* [DELPHI Coll.], *Phys. Lett.* **B471**, 460 (2000); G. Abbiendi *et al.* [OPAL Coll.], *Z. Phys.* **C16**, 423 (2000); A. Heister *et al.* [ALEPH Coll.], CERN-EP/2003-079.

[198] S. Chekanov *et al.* [ZEUS Coll.], *Phys. Lett.* **B583**, 231 (2004).

[199] C. Adler *et al.* [STAR Coll.] *Phys. Rev. Lett.* **87**, 082301 (2001); J. Adams *et al.*, *Phys. Rev. Lett.* **93**, 012301 (2004).

[200] N.M. Agababyan *et al.* [NA22 Coll.] *Phys. Lett.* **B422**, 359 (1998); A. Ster, T. Csörgő, B. Lörstad, *Nucl. Phys.* **A661**, 419 (1999); M. Csanád, T. Csörgő, B. Lörstad, A. Ster, *Acta Phys. Pol. B* **35**, 191 (2004); `nucl-th/0402037`; `hep-ph/0406042`.

[201] T. Csörgő, S. Hegyi, W.A. Zajc, *Eur. Phys. J.* **C36**, 67 (2004).

[202] H. Beker *et al.* [NA44 Coll.], *Z. Phys.* **C64**, 209 (1994); I.G. Bearden *et al.*, *Phys. Rev. Lett.* **87**, 112301 (2001); S.V. Afanasiev *et al.* [NA49 Coll.], *Phys. Lett.* **B557**, 157 (2003).

[203] J. Adcox *et al.* [PHENIX Coll.], *Phys. Rev. Lett.* **88**, 192302 (2002); S.S. Adler *et al.*, `nucl-ex/0401003`; B.B. Back *et al.* [PHOBOS Coll.], *J. Phys. G* **30**, S1049 (2004).

[204] B. Lörstad, O.G. Smirnova, *Proc. 7th Int. Workshop on Multiparticle Production*, eds. R.C. Hwa *et al.*, World Scientific, Singapore 1997, p. 42.

[205] T. Csörgő, J. Zimányi, *Nucl. Phys.* **A517**, 588 (1990); A. Bialas, K. Zalewski, *Acta Phys. Pol. B* **30**, 359 (1999).

[206] N.M. Agababyan *et al.* [NA22 Coll.], *Z. Phys.* **C68**, 229 (1995).

[207] P. Achard *et al.* [L3 Coll.], *Phys. Lett.* **B540**, 185 (2002).

[208] H. Bøggild *et al.* [NA44 Coll.], *Phys. Lett.* **B455**, 77 (1999); I.G. Bearden *et al.*, *Phys. Lett.* **B517**, 25 (2001).

[209] N.N. Aggarwal *et al.* [WA98 Coll.], *Phys. Rev. Lett.* **85**, 2895 (2000).

[210] J. Adams *et al.* [STAR Coll.], *Phys. Rev. Lett.* **91**, 262301 (2003).

[211] M.A. Braun, F. del Moral, C. Pajares, *Phys. Lett.* **B551**, 291 (2003).

[212] D. Miskowiec *et al.* [E877 Coll.], *Nucl. Phys.* **A590**, 473c (1995); M.A. Lisa *et al.* [E895 Coll.], *Phys. Lett.* **B496**, 1 (2000).

[213] J. Adams *et al.* [STAR Coll.], *Phys. Rev. Lett.* **93**, 012301 (2004).